A MULTIPORT APPROACH TO MODELING ELECTROMECHANICAL SYSTEMS

Thesis for the Degree of M. S.

MICHIGAN STATE UNIVERSITY

JOHN FRANCIS MOYNES

1976

ABSTRACT

A MULTIPORT APPROACH TO MODELING
ELECTROMECHANICAL SYSTEMS

By

John F. Moynes

In order to standardize the analysis, in particular computer analysis, of electromechanical systems, a multiport modeling approach on the electromechanical component level is used so that large systems may be assembled and studied directly.

Electromechanical component models are developed and compiled in a catalog. In addition, their configurations into systems and analysis by state-space techniques is demonstrated.

A MULTIPORT APPROACH TO MODELING ELECTROMECHANICAL SYSTEMS

by

John Francis Moynes

A THESIS

Submitted to
Michigan State University
in partial fulfillment of the requirements
for the degree of

MASTER OF SCIENCE

Department of Mechanical Engineering

1976

TABLE OF CONTENTS

LIST OF FIGURES

CHAPTER I

INTRODUCTION

A Multiport Approach to Electromechanical Components

1.1 Objectives

In an effort to aid the design and development of electromechanical systems, it is the objective of this thesis to establish a model catalog of some basic electromechanical components to serve as an initiative for further development in this area of design. The future goal is a computer library of electromechanical components that can be appropriately selected and assembled to form desired electromechanical systems for analysis and simulation. Further, it is the objective of this thesis to present the utility of the bondgraph approach to the problem of development, analysis, and simulation of electromcehanical system models. It should be noted that this thesis does not attempt to be comprehensive, but to demonstrate, by example, how models can be developed and systems assembled using bondgraph techniques.

Given a component, a port denotes any power* flow into or out of the component. Therefore, a component has as many external ports as it has external power* exchanges. A

---

*(or signal, if power is unimportant)

multiport component is one which has at least one external bond, where an external bond signifies the existence of a power flow. It is on this multiport level that modeling occurs. The multiport approach consists of modeling the energy storage, dissipation, transduction, and power exchanges of the electromechanical component on a lumped-parameter basis.

The versatility of the multiport approach is that its application is uniform in a variety of energy domains; therefore mixed energy domains are readily accomodated. Consequently, this approach lends itself to EM (electromechanical) components. In EM components, there is an energy conversion which transforms electrical power to mechanical (typically rotational) power, as shown by the generalized 2-port EM component in Figure 1-a, and its converse as shown in Figure 1-b. Note that the difference between Figures 1-a and 1-b is in the directions of the arrows, which mark the direction of positive power flow. v and i (voltage and current) are the electrical power variables and τ and ω (torque and angular velocity) are the mechanical power variables.

1.2 Organization

Using the bondgraph techniques as the principal tools of this construction, it is first necessary to model the essential parts prior to their assembly. Chapter II deals with the development of some basic EM component models which

typify the field of EM devices. The primary areas are solenoids, sensors, and motors.

Chapter III treats the assembly of component models into EM systems and outlines some of the types of analysis that may be employed using the mulitport approach. In order to display the pattern of the multiport approach, three distinct types of systems are represented.

1.3 Details

For those interested readers not familiar with bondgraphs and bondgraph computer analysis, informative references are "System Dynamics" by Karnopp and Rosenberg[1], the ASME "Journal of Dynamic Systems, Measurement, and Control"[2], and "A User's Guide to Enport-4" by R. C. Rosenberg.[3] The majority of the EM device background used in this work was drawn from a text by E. S. Charkey, "Electromechanical System Components"[4]. It should be noted that for those interested in the multiport approach to other mixed energy domains, there is a thesis by M. R. Ray titled "The Multiport Approach to Modeling Fluid Power Systems".[5]

CHAPTER II

A SAMPLE OF ELECTROMECHANICAL COMPONENTS

2.0 EM Transduction and Units

In a mixed energy domain there is always the harsh reality of maintaining a consistent set of units. Given the generalized electromechanical model of Figure 1, if this component is ideal, then the power in will equal the power out ($v \cdot i = \tau \cdot \omega$). This energy conversion typically occurs through a gyration effect, Figure 2-a, and care must be exhibited in the determination of the modulus (T) of the gyrator. The most direct solution to this possible problem is through the use of SI units, where both powers (volts x amps) and (newtonmeters x meters per second), are watts. This method allows the same modulus to be used in both transduction directions (i.e., electrical-to-mechanical and mechanical-to-electrical). However, if British or other units are to be used, then an alternate course must be taken. Ideally, there could be one gyrator with two moduli, one for voltage-to-velocity and one for torque-to-current transduction; see Figure 2-b. Realistically from the viewpoint of Enport, a digital computer program for the analysis of bondgraphs, the notion of two moduli to a passive gyrator is unacceptable. On the other hand, through the use of signal activation the

models in Figure 2-c, 2-d are acceptable and will yield consistent units so long as T_1 and T_2 are properly chosen. Then care must be taken to ensure that physical power is conserved.

2.1 Solenoids

The first of the EM components to be introduced is the solenoid. The solenoid is essentially nonlinear in the sense that it lacks a dynamic linear representation for gross motion. However, it can be linearized effectively.

The solenoid is basically a coil inductor with a moveable ferromagnetic core placed inside the coil along its axis, Figure 3. One port behaves as an electrical inductor while the other behaves as a mechanical spring. It is nonlinear because the position of the core has a nonlinear influence on the strength of the field, and the field strength determines the force on the core, thereby affecting the position of the core.

The describing equations of the solenoid will be developed in Section 3.1. Because of its dual energy storage nature, its ideal bondgraph equivalent element is the IC element, Figure 4. A more complete model deals with the electrical resistance of the coil, the inertia of the core, and the mechanical friction that the core will experience. Such a model is shown in Figure 5.

2.2 Sensors

Resistive, Inductive, and Capacitive types are three main electromechanical sensor classifications. Models will be developed for these classes. In addition, a tachometer model will be developed. It is assumed that all models operate within their physical constraints regions.

2.2.1 Resistive Sensors

In the resistive area there are strain gages and potentiometers. They both function by having a physical signal vary their resistance in an electrical circuit. The signal is the variable to be sensed, and the resulting change in current (or voltage) is an indication of its variation. Such sensors frequently are used for the determination of linear and angular displacements and acceleration (i.e., motion proportional to force).

On first pass, a generalized resistive sensor is shown below:

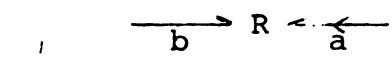

where activated bond a has the signal to be measured. The power variables on bond b have the following form:

$$e_b = \Phi_r(f_b, q_a)$$

where e_b is the effort (voltage) on bond b, f_b is the flow (current) on bond b, and q_b is the displacement (angle or position) signal from bond a. This nonlinear resistive sensor may be employed as a potentiometer measuring angular

displacement, as indicated below:

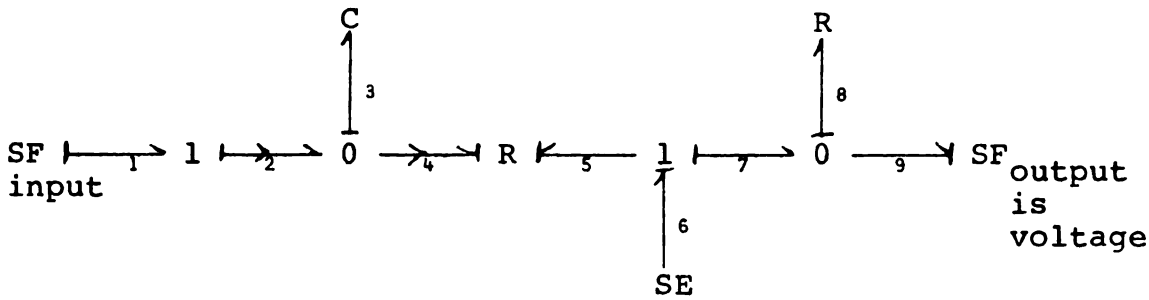

The source of flow from bond 1 represents angular velocity input. The capacitor (C3) serves as a symbolic integrator of the velocity input so that a displacement is sent to the R-Field. The remaining graph structure allows for a suitably-scaled voltage output.

Although R is a nonlinear element, it typically has linear characteristics over a wide range of practical use. Where this linear relationship exists, the model can be considerably simplified to a linear model:

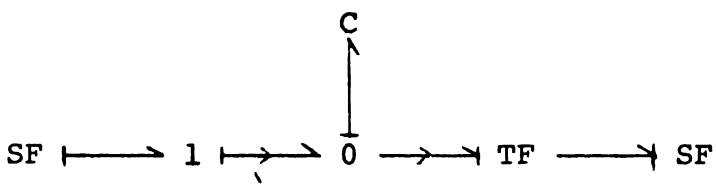

where the TF modulus has the desired scaling.

2.2.2 Inductive Sensors

Inductive sensors are generally used for determining linear displacement. They function on the principle of a moving ferromagnetic core in an electromagnetic field generated by a coil inductor, the basic IC component.

One widely used type of inductive sensor is the LVDT (Linear Variable Differential Transformer).[4] The LVDT

has three windings equally spaced on a cylindrical coil. The primary winding is the center coil, and the two adjacent coils are the secondary. A ferromagnetic core is placed axially inside the coils, creating a magnetic path among the three coils. When the primary winding is energized with an AC source, a voltage is induced in the secondary windings. Thus a position change by the core will result in a change in the output voltage. When the core is equidistant between the two secondary windings, the net output voltage is zero. A schematic of the device is shown in Figure 6.

In the bondgraph modeling of the LVDT, the IC element is again introduced. Though typically a two-port device, in this application it acts as a three-port device. A preliminary model for the LVDT is shown in Figure 7. This model neglects the resistance of the coils. A model with this taken into consideration is shown in Figure 8.

Note that the source of flow on bond 1 is the displacement input, and the source of flow on bond 9 is the voltage output. Bond 1 may be activated since the back force should typically be negligible on the systems it is designed to sense. Although this is a nonlinear model with dynamics, two factors should be taken into consideration. The first is that the time response of this sensor must be significantly faster than that of the variable it will be measuring. Secondly, though the

model is nonlinear, the input-output relationship over the typical usage range is linear. These two factors allow us to simplify the model considerably, such that the model in Figure 9 may be substituted. SF 1 is the displacement input variable, and the effort on bond 2 is treated as the voltage output. R is the desired scaling factor.

2.2.3 Capacitive Sensors

Like the previous sensors, capacitive types predominantly are used for measuring linear and angular displacement and velocities. These sensors usually operate in one of the two following ways; either a change in the area of the plates occurs while a fixed plate separation distance is maintained, or a change in the separation distance of two plates occurs while a constant area is maintained. A variable-area capacitor will be modeled as an example of a capacitive sensor.

This sensor is useful in determining angular velocities. There is a fixed plate and a moving plate, with the inertia of the moving plate assumed negligible. The moving plate is positioned to rotate past the fixed plate so that as it moves the common area between the two plates increases or decreases accordingly. This change in area affects the capacitance, C, so that C is a function of θ; see Figure 10,[4] p. 38. A bondgraph of this sensor is shown in Figure 11. As denoted by the complete, augmented graph, the variable area capacitor returns no significant

effort (i.e., torque) back on bond 1. However, the signal from bond 1 influences the capacitance on bond 2 in the following way:

$$C_2 = \frac{A(\theta)\varepsilon}{d}$$

where ε = dielectric constant, $A(\theta)$ = area (a function of θ), and d = distance between plates.

Although the model is nonlinear, if the response of the model is much faster than the velocity to be measured, then over a certain operating region the input-output relationship is assumed linear, and the model can be simplified to the model in Figure 12. R is the appropriate scaling factor, and the source of effort (i.e., voltage) accounts for the bias.

2.2.4 Tachometers

The last example of an electromechanical sensor is one of the most frequently used -- the tachometer. The tachometer produces a voltage output proportional to an angular velocity input. A schematic is shown in Figure 13. The bondgraph of the tachometer is represented in Figure 14, where I_1 is the rotary inertia of the input shaft and armature I_2 is the inductance of the armature coil, R_3 and R_4 represent the mechanical and electrical energy dissipations respectively, and the gyrator models the interaction of the rotating armature winding in a permanent magnetic field. (Bonds 5 and 8 are activated, Figure 14-b, because

any back effects should be negligible to the system with appropriate matchup of the tachometer to the system). Further, the inductances and resistances can be neglected since the dynamics of the tachometer should be much faster than the over-all system response. (Obviously, if this is not the case, the model argument is not useful). The final model for the tachometer is merely a gyrator with two activated bonds, Figure 14-c. R is the scaling factor.

Using the bond graph approach some rather complex sensors can be analyzed at a detailed level. However, they can be significantly simplified without losing their utility for restricted regions of operation.

2.3 Motors

The two major distinctions for motors fall under the headings AC powered or DC powered, but there are numerous types of motors under each heading. This section will deal with developing some basic types of DC motor models. The emphasis is on the DC motor rather then the AC motor, since the bondgraph development of the AC motor would tend to parallel that of the DC models in its apparent structure even thouth AC motors are considerably different in their magnetic field structure. Two good references for AC motor modeling are: The Unified Theory of Electromagnetic Machines, by M.G. Say[10] and a doctoral thesis by L.L. Evans[6] which has a bondgraph, multiport development of some AC motor models.

2.3.1 DC Motors

The four basic types of DC motors will be discussed: the permanent magnet, shunt, series, and compound types.

The basic motor model is a three-port device as shown in the word bondgraph of Figure 15. Note that if the power flows were changed in such a way that the rotational power was the input and the armature current was an output, then the model would be that of a generator instead of a motor.

The approach in modeling these motors will be to begin with an ideal model (i.e., linear, lossless) and to develop that model into a static and then a dynamic model. These classifications -- ideal, static, and dynamic -- are called orders and are the zeroth, first, and second orders, respectively.

Which electrical port is the input voltage depends on whether the motor is field-controlled or armature-controlled. In the development of the following models, all motors will be treated as armature-controlled.

The zeroth order model, Figure 16, takes an input voltage and outputs an angular velocity. The third port determines the gyrator modulation coefficient. The third port is typically treated as signal influenced, due to low field back-interaction. If the field signal is constant, the gyrator is linear rather than modulated. The linear zeroth order model is shown in Figure 17.

The next stage of model development is the static model. On this level dissipation effects are introduced

into the model. On the electrical side of the motor there are the resistances of both the armature and field windings. However, the resistance of the field winding has no significance in the armature-controlled, linearized gyrator model. Mechanically the motor has friction between the rotor and its bearings and there are air friction losses[7]. Each of these dissipative effects can be modeled as a single element as shown in Figure 18 which is the static motor model.

So far nothing has been assumed regarding the linearity of the R-Field. The model is good for both linear or nonlinear resistances. The electrical resistance is a linear relationship with a constant R term.

The mechanical resistance is nonlinear as a result of bearing friction, which looks like coulomb friction, Figure 19. The bearing friction is a constant regardless of the motor speed except at $\omega = 0$ where it is indeterminate. However, the frictional air loss is taken as linear where the torque loss is proportional to the speed. In practice, the mechanical resistance is treated simply as a linear function of the speed. However, this technique can be improved upon by going to a piecewise linear model as shown in Figure 20. The effort source models the constant loss of the bearing friction as long as the direction of the angular velocity does not change or go to zero. Once there has been a sign change in speed, the model becomes inoperative until there is a corresponding sign change on

the effort source.

The second order model (dynamic) is a rather complete physical model of the motor, which includes the components necessary to describe the major physical phenomenon associated with the motor.

The second model order includes the motor's inertia and the inductances of the windings of the rotor and stator. It is the wiring pattern of these windings that makes for the different types of motors. Model development thus far has been in the nature of a generalized DC motor model with a linearized gyrator. Now, with the inclusion of the motor's inertia and the inductances, which are assumed linear, the specific types of DC motors will be discussed. Schematics of the four different types of motors are shown in Figure 21.

The most common motor model is the permanent magnet motor, which has no field windings. Any DC motor model with a linearized gyrator will look like the permanent magnet motor model, Figure 22.

The remaining models, Figure 23, are simply permutations on the PM model, where all the models have modulated gyrators. Note that it is not necessary at this point to specify whether the resistances and inductances are linear or nonlinear. With these structural models available, it is only necessary to specify the type of motor and parameters desired in order that a motor can be included in an EM systems study. Further details on these models are

listed in the Catalog (Appendix A).

Once all these component models have been developed, it is just a matter of assembling the components into systems, inserting proper parameter values, and analyzing or simulating the system by standard bondgraph techniques. This is the subject of the next chapter.

CHAPTER III

MODELING OF ELECTROMECHANICAL SYSTEMS

3.1 Doorbell

In this chapter, three EM systems will be modeled. The first will be a doorbell, Figure 24. The component or word bondgraph model for the doorbell is shown in Figure 25. Substituting the appropriate bondgraph models for the components yields a suitable system bondgraph, Figure 26. Since the load of the system is in series with the inertia and damping of the solenoid, they simply add respectively. Likewise, the spring can be included in the C field. For analysis, the model must be fully augmented, which includes assigning power flows and causality, Figure 27.

The current version of Enport is linear, and therefore it will not accept a nonlinear IC component. However, it is still possible to model the system structure on Enport, and even though it will not yield state equations, it will assign causality and power flows. This is possible by use of a C field and a gyrator, Figure 28, which yield the proper port causalities.

Having a complete model, the next task is to derive the equations of state, where the state vector is: $[\tau \; x \; p]^t$, where τ is the electrical flux linkage, x is core displacement

and p is the momentum of the mass. It is now necessary to know the port characteristics of the IC element. On the electrical side the current is

$$i = \frac{\lambda}{L(x)}$$

where

$$L(x) = L_0 + A_e^{-\beta(x - x_0)^2}$$

A plot of L(x) versus x is shown in Figure 29-a,[8] where β [$\beta>0$] is the shape factor of the curve and x_0 is the magnetic center. L_0 and A determine minimum and maximum amplitudes of the inductance.

Since the IC element is energy-conservative, the mechanical force is determined as follows: integrating the power received over the time interval dt yields the net energy stored (W); differentiating this with respect to x will yield the mechanical force. The integral of the power is developed below:

$$W = \int_0^t (ei + fv)dt = \int_0^\lambda id\lambda + \int_0^x fdx = \int_0^\lambda \frac{\lambda}{L(x)} + \int_0^x fdx$$

where e = voltage, i = current, f = force, and v = velocity. This may be integrated along any path,[8] and the one chosen is shown in Figure 30, where for $\lambda = 0$, f will be zero. Thus

$$W = \frac{\lambda^2}{2L(x)}$$

and the force f is

$$f = \frac{dW}{dx} = \frac{\lambda^2 L'(x)}{L(x)^2}$$

where $L'(x) = \frac{dL(x)}{dx}$

A plot of L'(x) is shown in Figure 29-b.

With the IC relations, it is now possible to complete the state equations.

$$\dot{\lambda} = \frac{-R\lambda}{L(x)} + E(t)$$

$$\dot{x} = \frac{p}{m}$$

$$\dot{p} = \frac{\lambda^2}{2}\frac{L'(x)}{L^2(x)} - kx - \frac{b}{m}p$$

where R = 50Ω, E(t) = 100 volts, k = 2.4 newtons/meter, b = .01 newton-sec/meter, m = .02 newton-sec^2/meter(kg)

Parameters for these equations have been assumed, they are not from any specific model.

This set of simultaneous nonlinear differential equations can then be solved by making use of the digital computer.

3.2 PA System

The following EM system model is of a public address system. It is a simplified version; however, it could easily be evolved to a more sophisticated level depending upon one's needs. The basic system is depicted in Figure 31.

A condenser microphone operates on the principle of a moving-plate capacitor, and though a moving-plate capacitor is nonlinear, it can be effectively linearized around an operational equilibrium point.

The schematic model of the nonlinear microphone[8] and the fully augmented bondgraph are shown in Figure 32. SE 1

is the sound input force and bond 9 is the output port to the amplifier. The mechanical compliance (C4) of the moving plate can be included in the C-Field; however, it will be kept separate for the sake of clarity.

Assuming that the amplifier operates in a region of nonsaturation, the model for the amplifier is merely a transformer with the desired gain modulus and a suppressed back current, Figure 33; i.e., the microphone transmitts a signal to the amp.

In the schematic model, Figure 34,[8] of the permanent magnet loudspeaker, the gyrator models the ideal relation of the voice coil and cone assembly. The spring and dash-pot account for the cone's suspension, and the mass is that of the cone itself. The resistance and inductance are physical properties of the voice coil. This linear model example does not take into account the higher modes of vibration of the cone, as well as the acoustical properties of the enclosure. Therefore, the model is limited to a low frequency range for good predictive accuracy.

To fully account for the system, the driving load of the speaker should be included, i.e., the resistance and inertance of the air. These can be implicitly included in the speaker model in the R and I elements, respectively. However, for clarity the load will be placed outside the speaker model, as shown in Figure 35.

These separate component models can now be linked together by their common power bonds, Figure 36. As

previously stated, the 2 port C-Field is the only nonlinear element, and it can be linearized around some properly chosen operating point.

For a moving-plate capacitor, the capacitance is a function of x with the following relation:

$$C(x) = C_0 \frac{d_0}{d_0 + x}$$

where C_0 is the calculated capacitance, and d_0 is the distance between the plates when x is equal to zero. The port relations for the 2 port C-Field are found using the same energy approach as in the IC element shown previously (a reference to the complete development is found in footnote 8, page 292). The mechanical force is found to be

$$F = \frac{q^2}{C_0 d_0}$$

and the electrical voltage is:

$$E = \frac{d_0 + x}{C_0 d_0} q$$

Having these relations, the state equations for the microphone can be derived for the following state vector:

$$\begin{bmatrix} p \\ q \\ x \end{bmatrix}$$

where p is momentum; q, electric charge; and x, linear displacement.

The equations of state are:

$$\dot{p} = -kx - \frac{b}{m}p - \frac{q^2}{2C_0 d_0} + F(t)$$

$$\dot{q} = \frac{1}{\mathbb{R}}\left[E(t) - \frac{d_0 + x}{C_0 d_0} q\right] \qquad \} \text{ Equation 1}$$

$$\dot{x} = \frac{1}{m}p$$

where, $\mathbb{R} = R + R_L$. The values of the parameters are:

$k = 176{,}400$ newtons/meter

$m = .0010 \frac{\text{newton-sec}^2}{\text{meter}}$ (kg)

$d_0 = .000254$ meters

$b = 5.9$ newton-sec./meter

$C_0 = 10^{-6}$ farads

$R = 50.$ ohms

$E = 50.$ volts

To effectively linearize the state equations of the microphone, it is necessary to determine a stable equilibrium point in terms of x. The desired point will exist when the time derivatives are zero, and the eigenvalues indicate stability. Further it is desired that F(t) be set to zero, i.e., equilibrium pt. for no input. The resulting equations are:

$$kx = \frac{-q^2}{2C_0 d_0} \qquad \text{Equation 2}$$

$$E(t) = \frac{d_0 + x}{C_0 d_0} q \qquad \text{Equation 3}$$

where $E(t) = E_0$ (constant).

Now Equation 3 yields:

$$q = \frac{C_0 d_0 E_0}{d_0 + x}$$

By disposing of q from equation 2, the following relation for x exists:

$$kx = -\frac{C_0 E_0^2}{2d_0(1 + x/d_0)^2}$$

Substituting the parameter values and solving for x iteratively yields a stable equilibrium point at

$$\hat{x} = 3.9 \times 10^{-5} \text{ meters,}$$

With a corresponding charge of

$$\hat{q} = 5.9 \times 10^{-5} \text{ coulombs.}$$

In order to make the microphone suitable for linear analysis the microphone will be linearized around the equilibrium point $(\hat{x}, \hat{q})$ where x(t) and q(t) have the form:

$$\left.\begin{aligned} x(t) &= \hat{x} + x_0(t) \\ q(t) &= \hat{q} + q_0(t) \end{aligned}\right\} \text{ Equation 4}$$

where $x_0(t)$ and $q_0(t)$ are perturbations around the equilibrium point $(\hat{x}, \hat{q})$[8]. Substituting Equation 4 into Equation 1, and neglecting the higher order terms of q_0 and x_0 the following linearized equations are obtained:

$$\left.\begin{aligned} \dot{p} &= F(t) - kx_0 - \frac{b}{m}p - \frac{\hat{q}}{C_0 d_0} q_0 \\ \dot{q}_0 &= -\frac{1}{IR}\left[((d_0 + \hat{x})/C_0 d_0) q_0 + \frac{\hat{q}}{C_0 d_0} x_0 \right] \\ \dot{x}_0 &= \frac{p}{m} \end{aligned}\right\} \text{ Equation 5}$$

In matrix notation the linearized equations have the form:

$$\begin{bmatrix} \dot{p} \\ \dot{q}_0 \\ \dot{x}_0 \end{bmatrix} = \begin{bmatrix} -\frac{b}{m} - \frac{\hat{q}}{C_0 d_0} & -k \\ 0 - \frac{(d_0 + \hat{x})}{IRC_0 d_0} & -\frac{\hat{q}}{IRC_0 d_0} \\ \frac{1}{m} & 0 \qquad 0 \end{bmatrix} \begin{bmatrix} p \\ q_0 \\ x_0 \end{bmatrix} + \begin{bmatrix} 1 \\ 0 \\ 0 \end{bmatrix} F(t),$$

Equation 6.

The linearized microphone then has the bondgraph shown in Figure 37. Note that the electrical source of effort has been eliminated and the capacitance of the spring has been included in the C-Field. The C-Field is defined by the following matrix relation:

$$\begin{bmatrix} f \\ e \end{bmatrix} = \begin{bmatrix} k & \frac{\hat{q}}{C_0 d_0} \\ \frac{\hat{q}}{C_0 d_0} & \frac{d_0 + \hat{x}}{C_0 d_0} \end{bmatrix} \begin{bmatrix} x_0 \\ q_0 \end{bmatrix} \qquad \text{Equation 7}$$

The fact that the off-diagional terms are equal implies that it is a conservative energy field.[1]

The final linear system bondgraph, Figure 38, is then a fifth order model, and while quite awkward to solve by hand, it is readily simulated by a digital computer.

3.3 Feed-forward Position Control

The final example was taken from a paper by Kulkarni and Chary[9]. It is a feed-forward position control servo-mechanism. In their paper a solution was generated through several assumptions and by use of signal flow graphs. Using the same general model and assumptions, the bondgraph approach will be applied in an attempt to generate the same solution. In rather mixed notation a model of the system is shown in Figure 39.

The input shaft displacement is detected by a sensor which transmits an electrical signal which is then compared with the output shaft displacement. The comparison of the

two results in an error signal. The error signal (in this study all electrical signals are voltages) is sent to the two sybsystems. Each subsystem consists of a sensor, amplifier, DC motor and appropriate gearing. In the system, there are two delays. Since these were ignored in the original paper, for the purpose of comparison they will be treated similarly here. However, it should be pointed out that the inclusion of these delays would pose no problem to the bondgraph approach.

One error signal goes directly to an amplifier which operates motor one, a DC, field-controlled motor. The position response of motor one with respect to the load is then fed back, via another sensor, to its amplifier, the comparator, and to a summer which is just ahead of the second subsystem. The original error signal and first subsystem response are appropriately summed with the resulting signal controlling subsystem two. Subsystem two has the same behavior as subsystem one. Both subsystems one and two have the same parameters, though this need not be the case.

In the model, it is assumed that there is no shaft compliance and that the two gear trains are ideal (i.e., lossless, mechanical transformers). Should it be necessary, shaft compliance and non-ideal gear trains may be readily and easily included in the complete model. Since the armature current of each motor is constant, the armature port effect is contained in the motor model, (i.e., the appropriate gyrator). The motor model is that of a DC shunt

motor. The complete device-level bondgraph of the system with the appropriate power and signal flows is shown in Figure 40.

The sensors are position sensors, where the angular velocity is integrated to angular position and then transformed to a voltage signal, Figure 41. The comparator is merely part of the bondgraph junction structure, and the amplifier is the linear model developed previously, assuming no saturation. To complete the model, the load consists of a rotary inertia with damping. It should be noted that the load is positioned by the sum of the velocities of the two subsystems as signified by bonds A and B at the zero junction in Figure 40.

This model will now be modified into a hybrid model, Figure 42. This is not necessary from a bondgraph point of view, but this was the manner of treatment in the original paper and for the purpose of comparison it will be followed.*

In the hybrid model the inertia and damping of the load are scaled and included in the motor model of each subsystem. The reason for this hybridization is straight forward. The true model contains three rotary inertias any two of which may be treated as independent state variables with the third being dependent. Rather than carry the complications of a dependent variable in the model,

---

*The input signal and sensor are compounded and treated as a source of effort.

Kulkarni and Chary modeled the three inertias as two, where the load is taken into account by altering the inertia (J) and damping coefficient (b) of each motor in subsystem one and two. Consequently, these two inertias both lead to independent state variables.

For this model change to be correct, the following conditions must be true. When subsystem one acts upon the load there exists, during that time interval, no coupling between the load and subsystem two. Further, when subsystem two acts upon the load, in another time interval, there is no coupling between the load and subsystem one.

In terms of the bondgraph approach (for ease and clarity the TFs and Rs have been dropped) the model in Figure 43-a was said to be dualized by the model in Figure 43-b, with appropriate changes to M_1 and M_2. Although this may be a reasonable assumption, in actuality, it is not a correct dual model, as will be shown.

The correct model of Figure 43-a, Figure 43-c, is an implicit I-Field which exhibits the cross coupling of bonds (1) and (2). The matrix relationship:

$$\begin{bmatrix} v_1 \\ v_2 \end{bmatrix} \quad \begin{bmatrix} i_{11} & i_{12} \\ i_{21} & i_{22} \end{bmatrix} \begin{bmatrix} p_1 \\ p_2 \end{bmatrix}$$

p = momentum, v = velocity, is derived below via transmission matrix techniques.

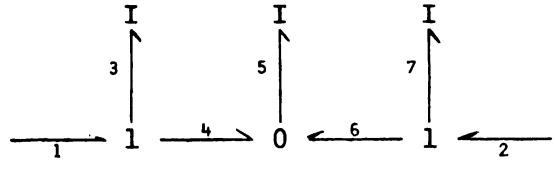

These techniques are described in more detail later in the reference paper. For the model below, the following relations hold (where e is force, f is velocity, and s is used in the context of LaPlace transforms):

$$\begin{bmatrix} e_1 \\ f_1 \end{bmatrix} = \begin{bmatrix} 1 & m_3 s \\ 0 & 1 \end{bmatrix} \begin{bmatrix} e_4 \\ f_4 \end{bmatrix}$$

$$\uparrow$$
$$I_A$$

$$\begin{bmatrix} e_4 \\ f_4 \end{bmatrix} = \begin{bmatrix} 1 & 0 \\ \frac{1}{m_5 s} & -1 \end{bmatrix} \begin{bmatrix} e_6 \\ f_6 \end{bmatrix}$$

$$\uparrow$$
$$I_B$$

$$\begin{bmatrix} e_6 \\ f_6 \end{bmatrix} = \begin{bmatrix} 1 & -m_7 s \\ 0 & 1 \end{bmatrix} \begin{bmatrix} e_2 \\ f_2 \end{bmatrix}$$

$$\uparrow$$
$$I_C$$

These matrix relations may be substituted to yield the relationship between $[e_1 \ f_1]^t$ and $[e_2 \ f_2]^t$:

$$\begin{bmatrix} e_1 \\ f_1 \end{bmatrix} = I_A \times I_B \times I_C \begin{bmatrix} e_2 \\ f_2 \end{bmatrix}$$

$$= \begin{bmatrix} \frac{m_5 + m_3}{m_5} & -\frac{(m_7 m_5 + m_7 m_3 + m_3 m_5)s}{m_5} \\ \frac{1}{s m_5} & \frac{-m_7 + m_5}{m_5} \end{bmatrix} \begin{bmatrix} e_2 \\ f_2 \end{bmatrix}$$

This can then be placed in the form:

$$\begin{bmatrix} f_1 \\ f_2 \end{bmatrix} = \begin{bmatrix} \frac{m_4 + m_5}{m_7 m_5 + m_5 m_3 + m_3 m_7} & \frac{-m_5}{m_7 m_5 + m_5 m_3 + m_3 m_7} \\ \frac{-m_5}{m_7 m_5 + m_5 m_3 + m_3 m_7} & \frac{-(m_5 + m_3)}{m_7 m_5 + m_5 m_3 + m_3 m_7} \end{bmatrix} \begin{bmatrix} \frac{e_1}{s} \\ \frac{e_2}{s} \end{bmatrix}$$

Since:

$$e_1 = \frac{dp_1}{dt} \text{ and } e_2 = \frac{dp_2}{dt}$$

or in terms of LaPlace:

$$e_1 = sp_1 \text{ and } e_2 = sp_2$$

Then:

$$\begin{bmatrix} f_1 \\ f_2 \end{bmatrix} = \mathfrak{I} \begin{bmatrix} p_1 \\ p_2 \end{bmatrix}$$

Not only does the existence of the i_{12}, i_{21} terms show the cross coupling, but the fact that they are equal proves that the I-Field is energy conservative, which we would expect from physical reasoning.

With the development of suitable models for the multiport components, it is merely a matter of substituting them into the device level multiport model, Figure 42, to obtain the complete model, Figure 44. Figure 45 is then the complete system model fully augmented.

In the original study, the motor field inductances were considered negligible. Accordingly, those components may be deleted from Figure 45, leaving the final system model. Having obtained an analogous model to that of Kulkarni and Chary, there are now three bondgraph techniques that can be used to generate a solution for the transfer function between the input and the output. One technique consists of generating the state equations, whereby the transfer function is obtained through the application of matrix techniques. Another technique is the transmission

matrices approach, and the last technique is the use of computer analysis which uses the computer program, Enport 4.2. In an effort to illustrate a manual approach, only the first two techniques will be applied.

The state equations in matrix form are:

$$\begin{bmatrix} \dot{p}_1 \\ \dot{x}_2 \\ \dot{p}_3 \\ \dot{k}_4 \end{bmatrix} = \begin{bmatrix} -b_5/J_1 & -r_{30}k_A k_{26}/R_6 & 0 & 0 \\ n/J_1 & 0 & 0 & 0 \\ 0 & -r_{22}k_A k_{26}/R_8 & -b_0/J_3 & -r_{22}k_A k_{17}/R_8 \\ 0 & 0 & n/J_3 & 0 \end{bmatrix} \begin{bmatrix} p_1 \\ x_2 \\ p_3 \\ x_4 \end{bmatrix}$$

$$+ \begin{bmatrix} r_{30}k_A/R_6 \\ 0 \\ r_{22}K_A/R_8 \\ 0 \end{bmatrix} E(t)$$

where p_1 is the angular momentum of motor one, x_2 is the geared shaft position of motor one, and p_3 and x_4 have the same respective designations, but for motor two. E(t) is the input variable, i.e., the desired shaft position. The output variable, θ (the output shaft position), is the summation of the x_2 plus x_3.

Using LaPlace techniques and substituting the numerical parameters, Figure 46, the $(SI - A)^*$ matrix is:

$$\begin{bmatrix} s + 1 & 40 & 0 & 0 \\ -100 & s & 0 & 0 \\ 0 & 40 & s + 1 & 40 \\ 0 & 0 & -100 & s \end{bmatrix}$$

The transfer function for $\theta(s)/E(s)$ is determined by

---

*Where $\dot{x} = \tilde{A}x + \tilde{B}u$

solving for x_2 and x_4 via Cramer's Rule:

$$\frac{\theta(s)}{E(s)} =$$

$$\frac{\left|\begin{bmatrix} s+1 & 40 & 0 & 0 \\ -100 & 0 & 0 & 0 \\ 0 & 40 & s+1 & 40 \\ 0 & 0 & -100 & s \end{bmatrix}\right| + \left|\begin{bmatrix} s+1 & 40 & 40 & 0 \\ -100 & s & 0 & 0 \\ 0 & 40 & 40 & 40 \\ 0 & 0 & 0 & s \end{bmatrix}\right|}{|SI - A|}$$

Taking the determinant yields:

$$\frac{\theta(s)}{E(s)} = \frac{8000s^2 + 8000s + 16\times10^6}{s^4 + 2s^3 + 8001s^2 + 8000s + 16\times10^6}$$

which is the same relation obtained in the original paper.

Using the transmission matrix approach, a transfer function may be obtained without generating the state equations. A transmission matrix (M) has the form whereby the power variables (e_i, f_i) of one bond of a two port device are related to the power variables of the other bond of the two port device, an example of which is shown below:[1]

$$\xrightarrow[f_1]{e_1} M \xrightarrow[f_2]{e_2} \quad \begin{bmatrix} e_1 \\ f_1 \end{bmatrix} = \begin{bmatrix} m_{11} & m_{12} \\ m_{21} & m_{22} \end{bmatrix} \begin{bmatrix} e_2 \\ f_2 \end{bmatrix}$$

The transmission matrix for subsystem one is developed in the following stages. Subsystem One:*

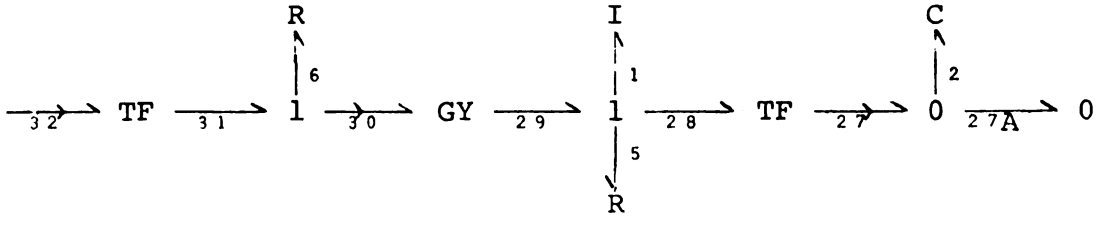

*Bond 27A and the extra zero are included for ease of handling.

$$\xrightarrow[32]{} \text{TF} \xrightarrow[31]{} \begin{bmatrix} e_{32} \\ f_{32} \end{bmatrix} = \begin{bmatrix} 1/n & 0 \\ 0 & 0^{*} \end{bmatrix} \begin{bmatrix} e_{31} \\ f_{31} \end{bmatrix}$$

$$M_{32-31}$$

$$\xrightarrow[31]{} \underset{\uparrow 6}{\overset{R}{1}} \xrightarrow[30]{} \begin{bmatrix} e_{31} \\ f_{31} \end{bmatrix} = \begin{bmatrix} 0 & R \\ 0^{*} & 1 \end{bmatrix} \begin{bmatrix} e_{30} \\ f_{30} \end{bmatrix}$$

$$M_{31-30}$$

$$\xrightarrow[30]{} \text{GY} \xrightarrow[29]{} \begin{bmatrix} e_{30} \\ f_{30} \end{bmatrix} = \begin{bmatrix} 0 & 0^{*} \\ 1/r & 0 \end{bmatrix} \begin{bmatrix} e_{29} \\ f_{29} \end{bmatrix}$$

$$M_{30-29}$$

$$\xrightarrow[29]{} \underset{5 \downarrow}{\overset{I}{\underset{R}{I}}} \overset{\uparrow 1}{} \xrightarrow[28]{} \begin{bmatrix} e_{29} \\ f_{29} \end{bmatrix} = \begin{bmatrix} 1 & R_5 + I_1 s \\ 0 & 1 \end{bmatrix} \begin{bmatrix} e_{28} \\ f_{28} \end{bmatrix}$$

$$M_{29-28}$$

$$\xrightarrow[28]{} \text{TF} \xrightarrow[27]{} \begin{bmatrix} e_{28} \\ f_{28} \end{bmatrix} = \begin{bmatrix} 0^{*} & 0 \\ 0 & 1/n \end{bmatrix} \begin{bmatrix} e_{27} \\ f_{27} \end{bmatrix}$$

$$M_{28-27}$$

$$\xrightarrow[27]{} \underset{\uparrow 2}{\overset{C}{0}} \xrightarrow[27A]{} \begin{bmatrix} e_{27} \\ f_{27} \end{bmatrix} = \begin{bmatrix} 0^{*} & 0 \\ Cs & 1 \end{bmatrix} \begin{bmatrix} e_{27A} \\ f_{27A} \end{bmatrix}$$

$$M_{27-27A}$$

$$M_{32-27A} = M_{32-31} \times M_{31-30} \times M_{30-29} \times M_{29-28} \times M_{28-27} \times M_{27-27A}$$

---

*Zero due to activation.

Hence:

$$M_{32-27A} = \begin{bmatrix} \frac{R_6C_2s(R_5 + I_1s)}{nn\bar{r}} & \frac{R_6(R_5 + I_1s)}{nn\bar{r}} \\ 0 & 0 \end{bmatrix}$$

This same manner yields:

$$M_{15-19A} = \begin{bmatrix} \frac{R_8C_4s(R_7 + I_3s)}{nn\bar{r}} & \frac{R_8(R_7 + I_3s)}{nn\bar{r}} \\ 0 & 0 \end{bmatrix}$$

$$M_{16-17} = \begin{bmatrix} 1/n & 0 \\ 0 & 0 \end{bmatrix} \qquad M_{34-26} = \begin{bmatrix} 1/n & 0 \\ 0 & 0 \end{bmatrix}$$

The graph with transmission matrices is:

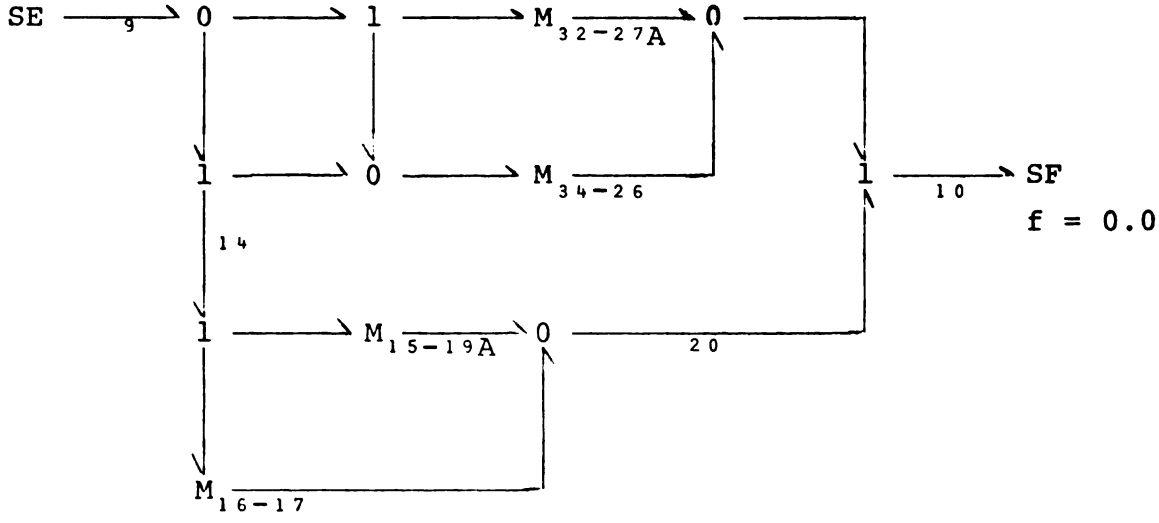

Due to the nature of the activated bonds in M_{16-17}

$$M_{14-20} = M_{15-19_A} + M_{16-17}$$

$$= \begin{bmatrix} 1 + \frac{R_8C_4s(R_7 + I_3s)}{nn\bar{r}} & \frac{R_8(R_7 + I_3s)}{nn\bar{r}} \\ 0 & 0 \end{bmatrix}$$

From the bondgraph in Figure 47, the transfer function for e_{10}/e_9 is obtained.

All three transmission matrices are 1 x 2, since row two is null for each matrix due to activation. The flow variables are deleted, in manipulating the matrices according to junction structure.*

$$e_9 = e_{11} = e_{32} + e_{33} = M_{32}e_{27A} + M_{34}M_{32}e_{27A}$$

$$e_9 = (M_{32} + M_{34}M_{32})(e_{10} - e_{20}) \qquad \text{Equation 8}$$

$$e_9 = e_{12} = e_{14} + e_{13} = M_{14}e_{20} + M_{34}(e_{10} - e_{20})$$

$$e_9 = (M_{14} - M_{34})e_{20} + M_{34}e_{10} \qquad \text{Equation 9}$$

From Equation 9 comes the relationship:

$$\frac{e_9 - M_{34}e_{10}}{M_{14} - M_{34}} = e_{20} \qquad \text{Equation 10}$$

Using Equation 10 for e_{20} in Equation 8 yields:

$$e_9 = (M_{32} + M_{34}M_{32})\left(e_{10} - \frac{e_9 - M_{34}e_{10}}{M_{14} - M_{34}}\right)$$

Simplifying:

$$\left[1 + \frac{M_{32} + M_{34}M_{32}}{M_{14} - M_{34}}\right] e_9 =$$

$$\left[M_{32} + M_{34}M_{32} + \frac{M_{34}(M_{32} + M_{34}M_{32})}{M_{14} - M_{34}}\right] e_{10}$$

Substituting the numerical values into the transmission matrices and the transmission matrices into the above equation yields the following function:

$$\frac{e_{10}}{e_9} = \frac{8000s^2 + 8000s + 16x10^6}{s^4 + 2s^3 + 8001s^2 + 8000s + 16x10^6},$$

which is the same as in the original paper.

---

*M's have shortened form, M_{A-B} becomes M_A.

At this point two investigative paths are available. One would be to use the transfer function in a frequency response study, making use of available computer programs. The other would be to run some simulations on Enport to study its overall system behavior to some given inputs.

FIGURES

Figure 1

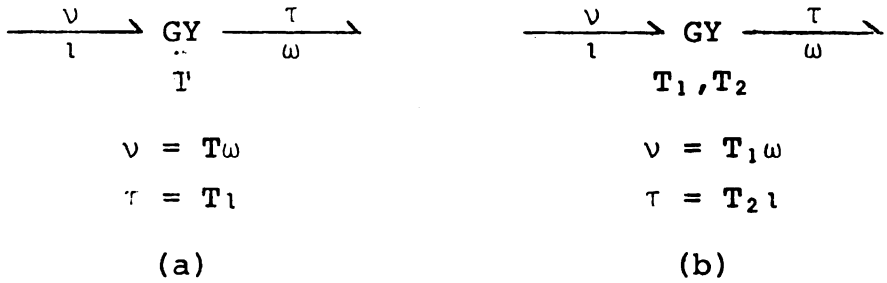

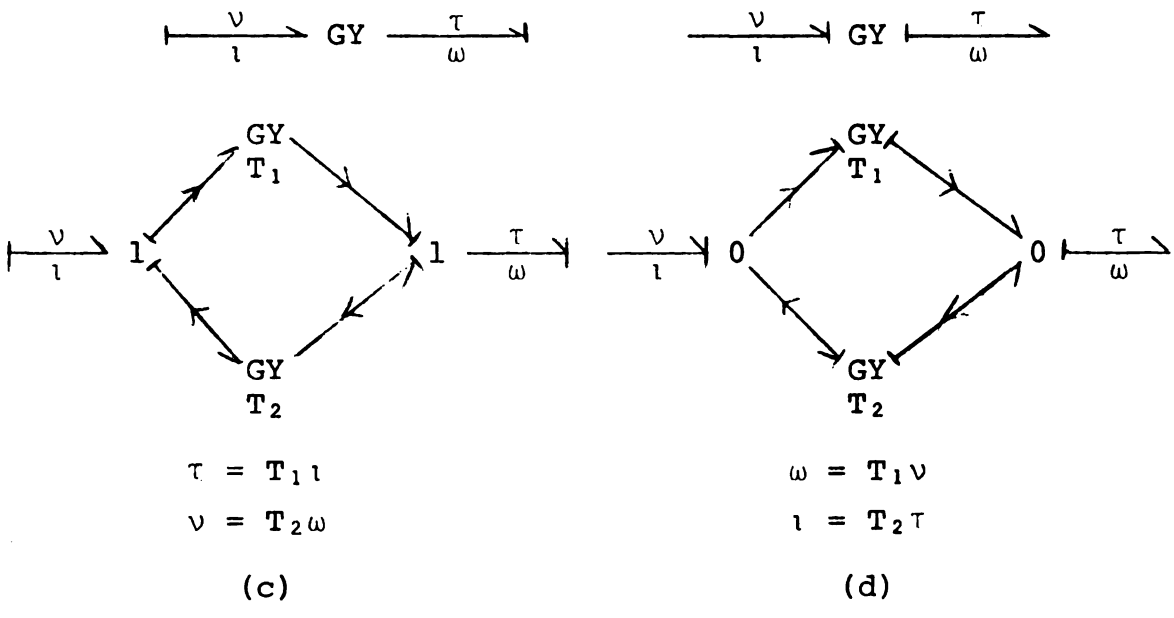

Figure 2

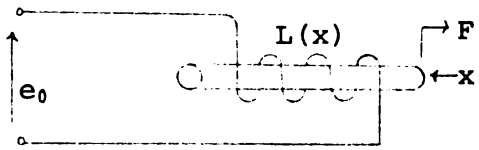

Solenoid

Figure 3

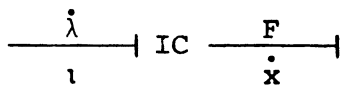

IC Component with Prefered Causality

Figure 4

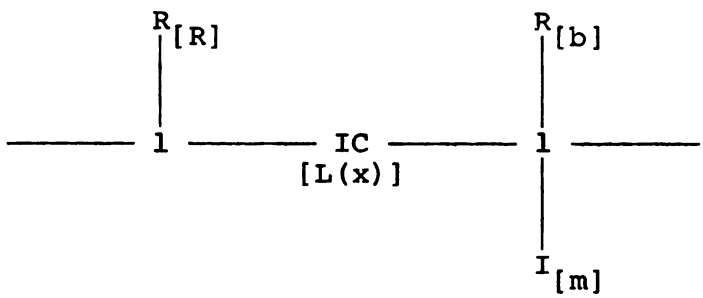

Complete Sensor Model

Figure 5

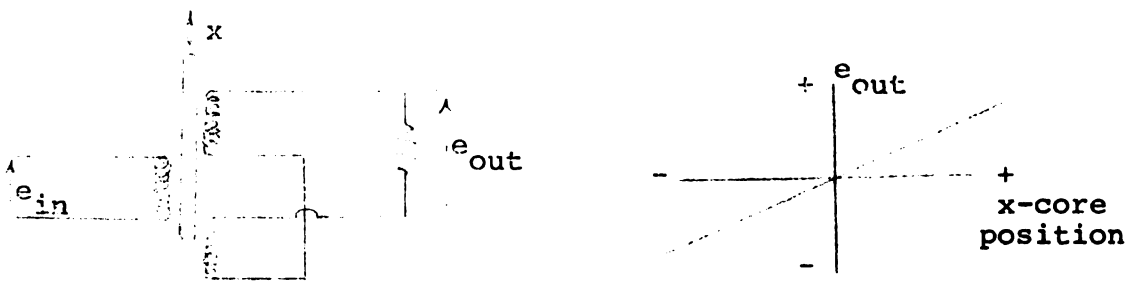

Schematic, LVDT

Figure 6

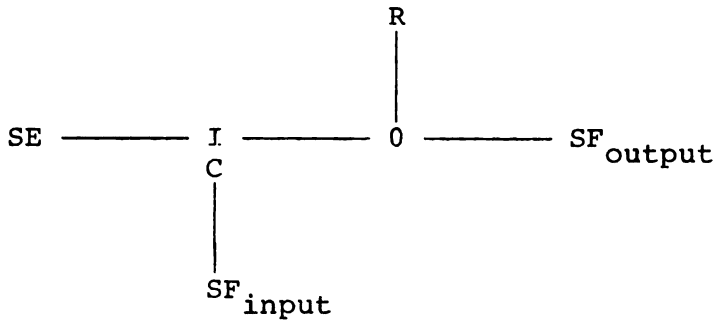

LVDT, Preliminary Model

Figure 7

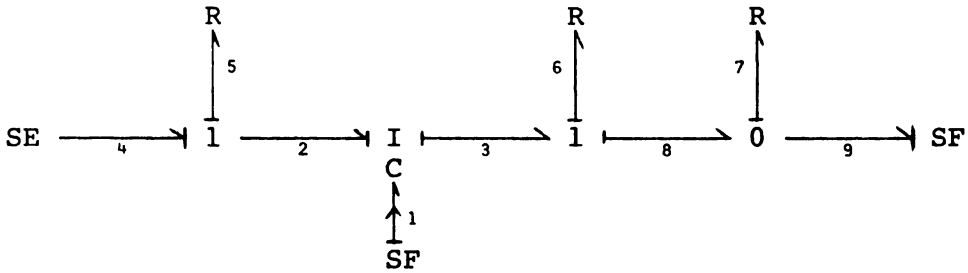

Complete Augmented LVDT Model

Figure 8

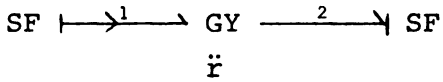

Simplified LVDT

Figure 9

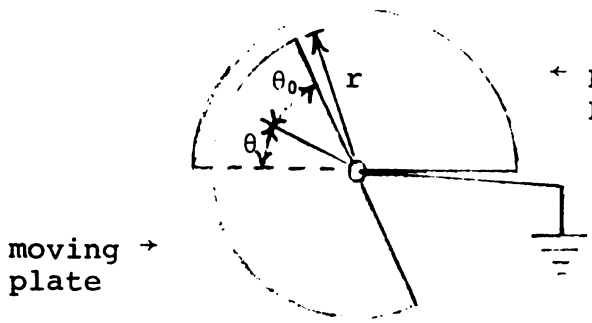

$$C(\theta) = \frac{A(\theta)}{d}$$

where $A(\theta) = \frac{r^2}{2}(\theta_0 + \theta)$

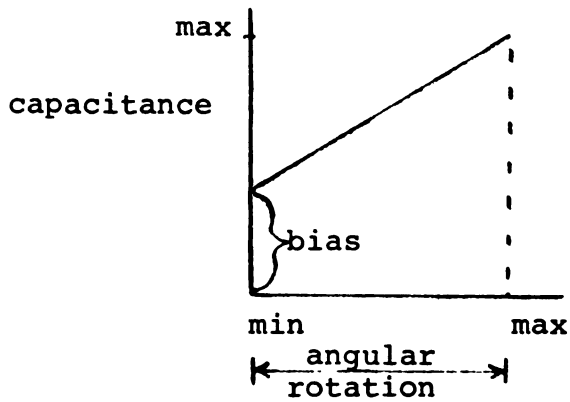

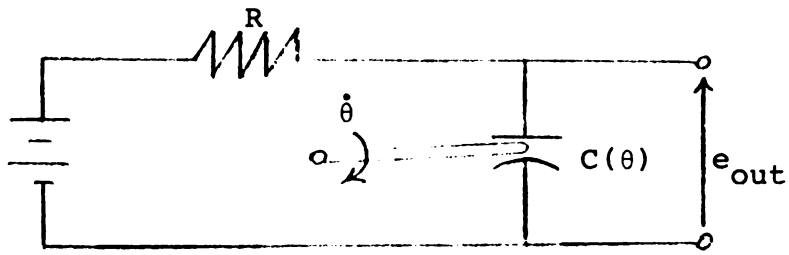

Schematic For Variable Area Capacitive Transducer

Figure 10 [ref. (4), p. 58]

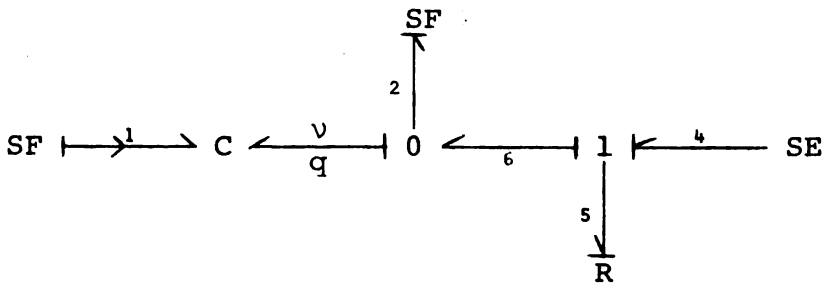

Complete Bond Graph of
Capacitive Transducer

Figure 11

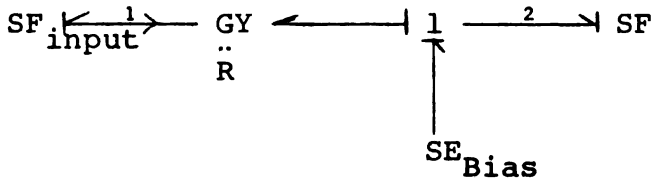

Simplified Capacitive Sensor

Figure 12

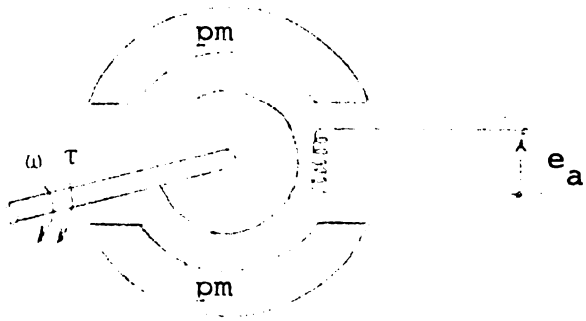

Tachometer Schematic

Figure 13

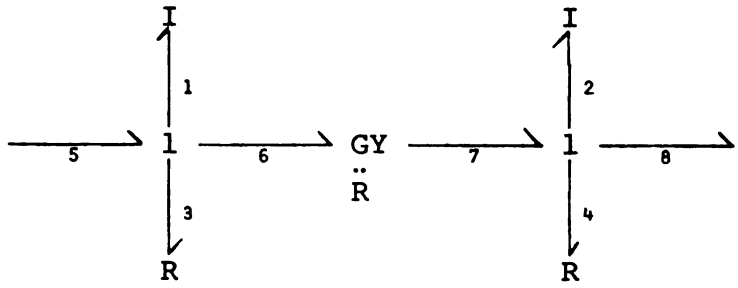

(a)

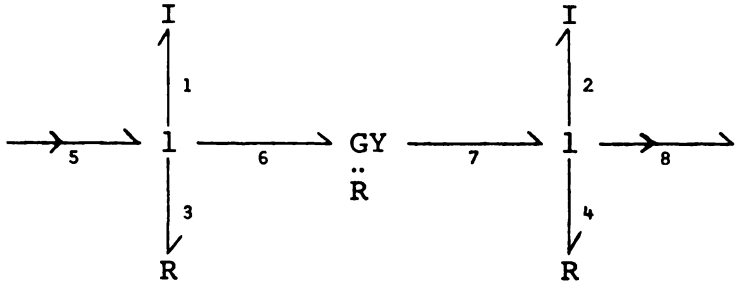

(b)

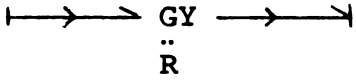

(c)

Bond Graph Development of Tachometer

Figure 14

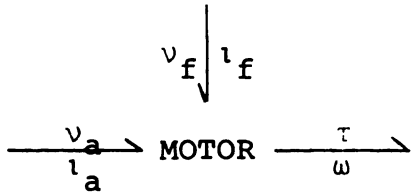

Word Bond Graph

Figure 15

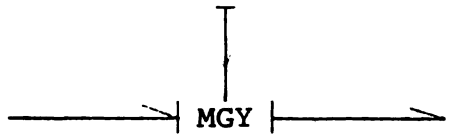

General Zeroth Order Motor Model

Figure 16

Linear Zeroth Order Motor Model

Figure 17

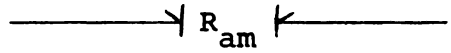

Static Motor Model

Figure 18

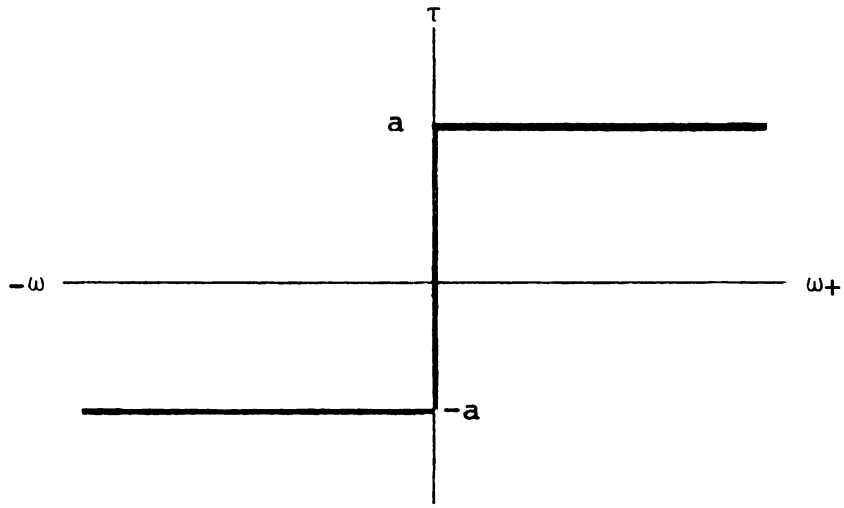

Bearing Friction

Figure 19

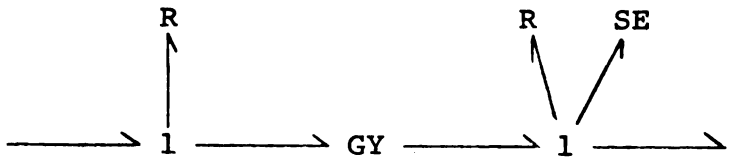

Piecewise Linear Static Model

Figure 20

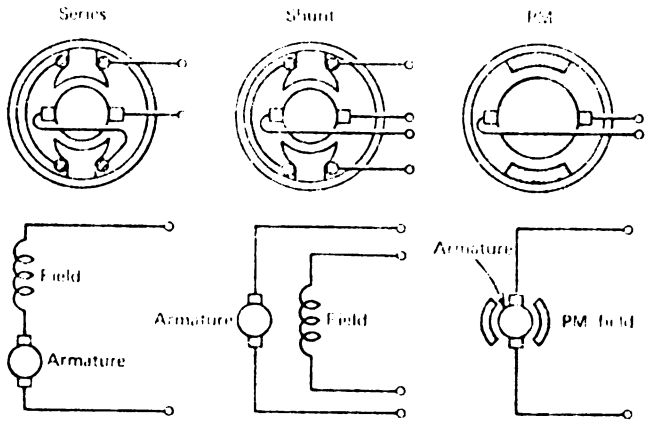

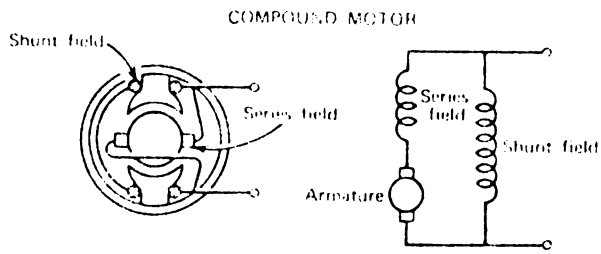

DC Motor Schematic

Figure 21

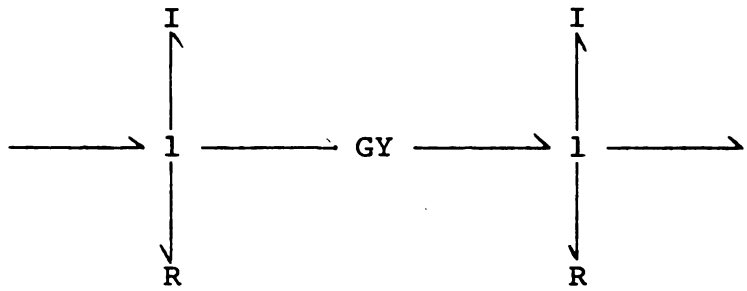

Complete Permanent Magnet Motor Model

Figure 22

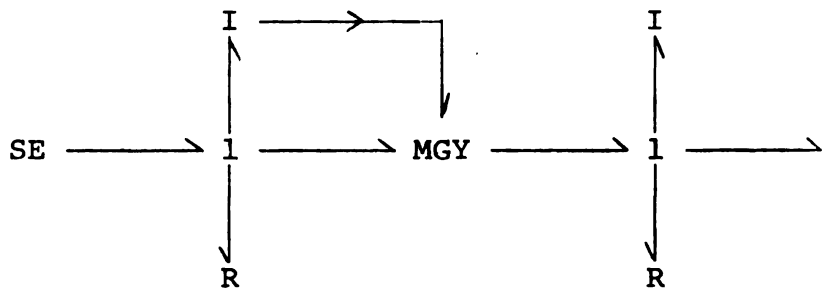

Series Motor Model
(a)

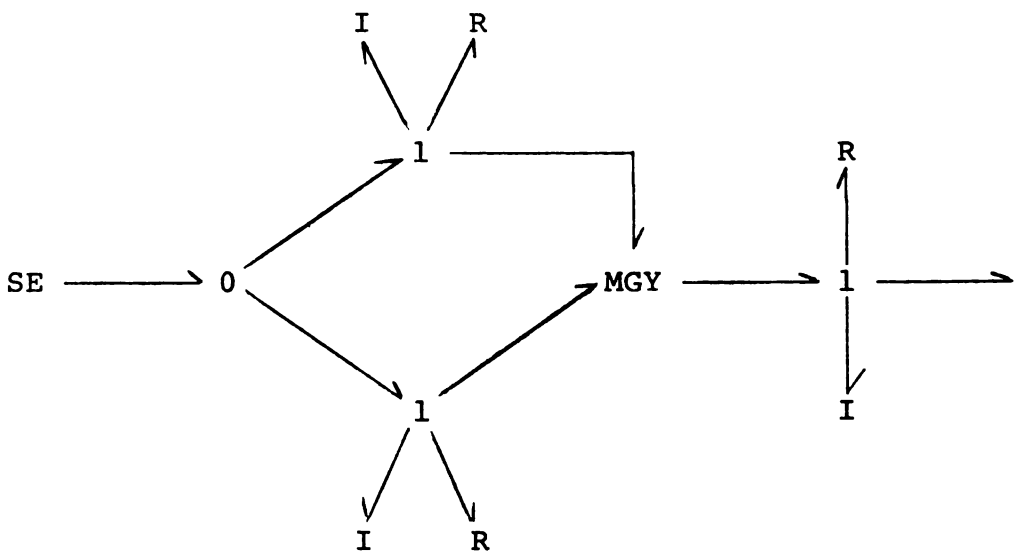

Compound Motor Model
(b)

Figure 23

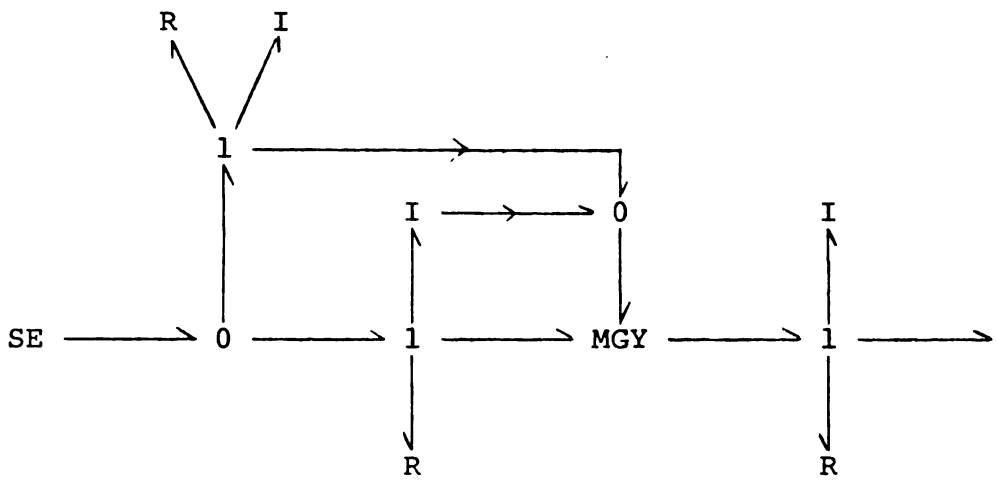

Compound Motor Model

(c)

Figure 23 - continued

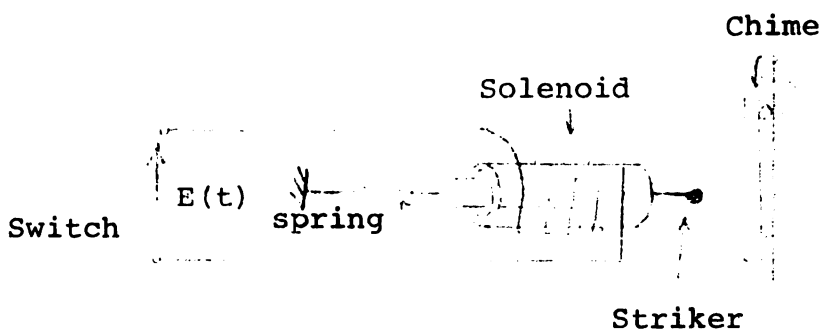

Door Bell

Figure 24

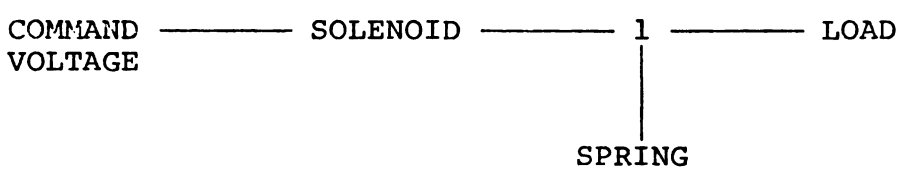

Word Bond Graph

Figure 25

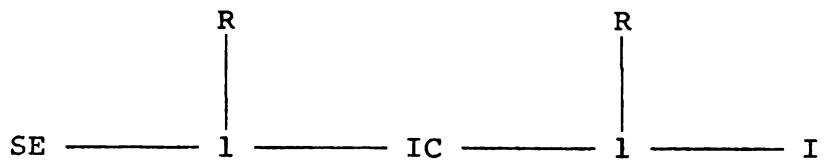

System Model

Figure 26

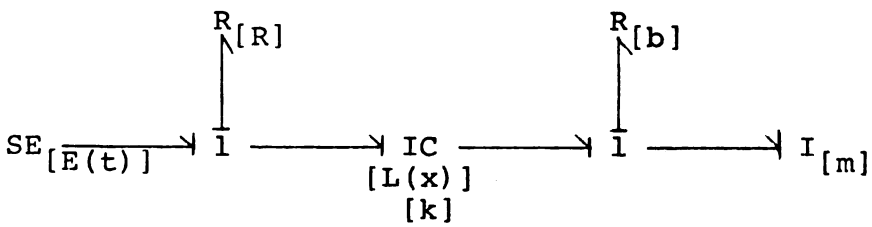

Fully Augmented System Model

Figure 27

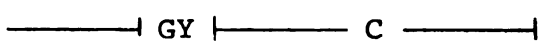

IC Linear Representation

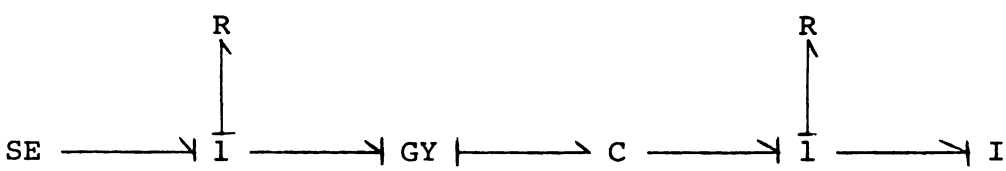

Enport Doorbell Model

Figure 28

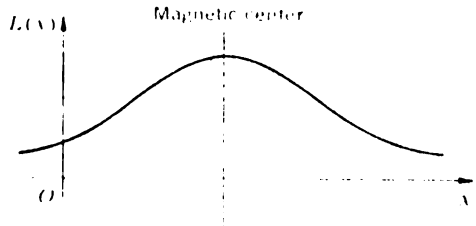

(a)

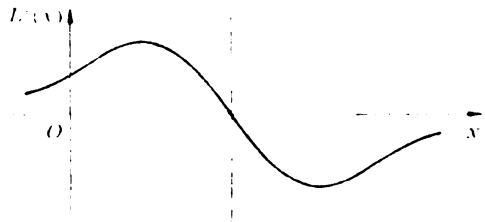

(b)

Figure 29

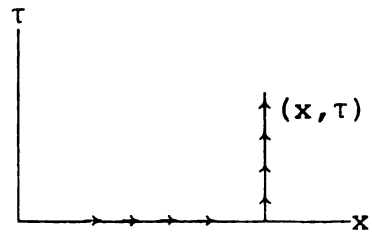

Figure 30

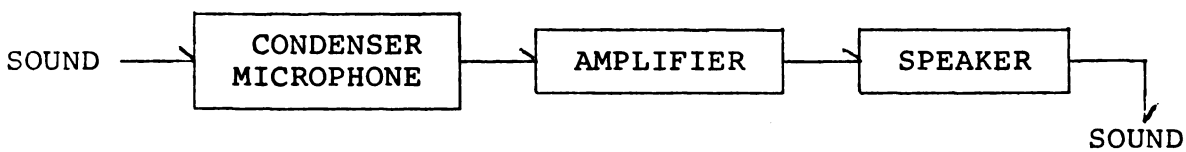

P. A. System

Figure 31

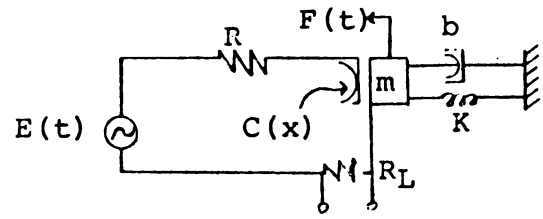

Mircophone Schematic

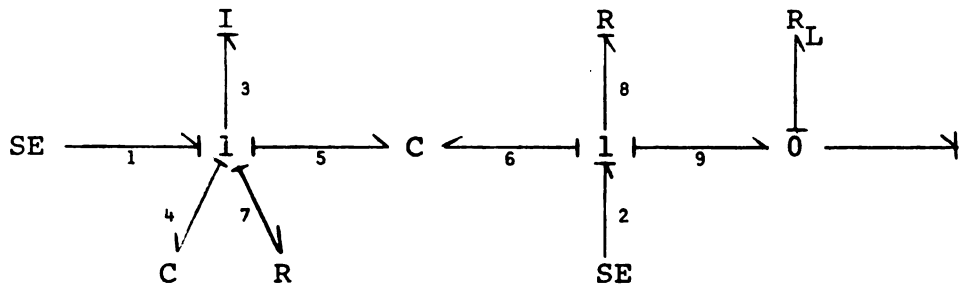

Fully Augmented Bond Graph of Condenser Microphone

Figure 32

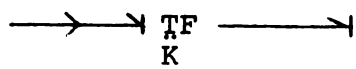

Linear Amplifer Model

Figure 33

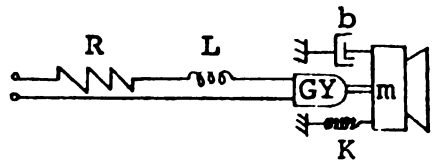

Loudspeaker Schematic

Figure 34

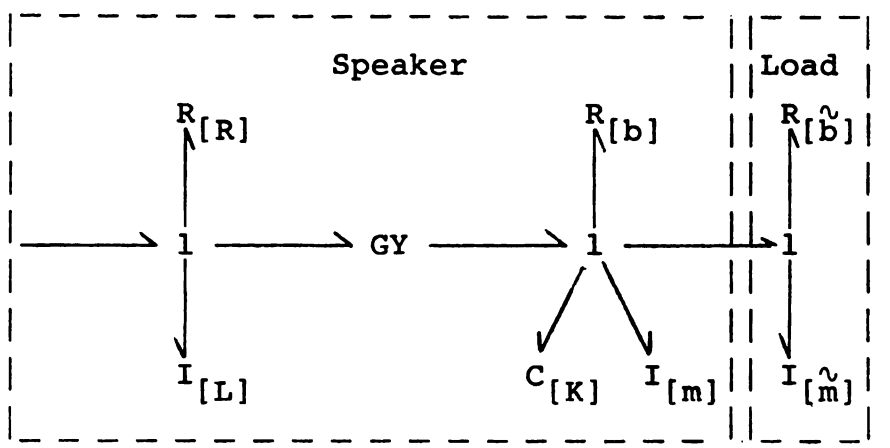

Loudspeaker Bond Graph

Figure 35

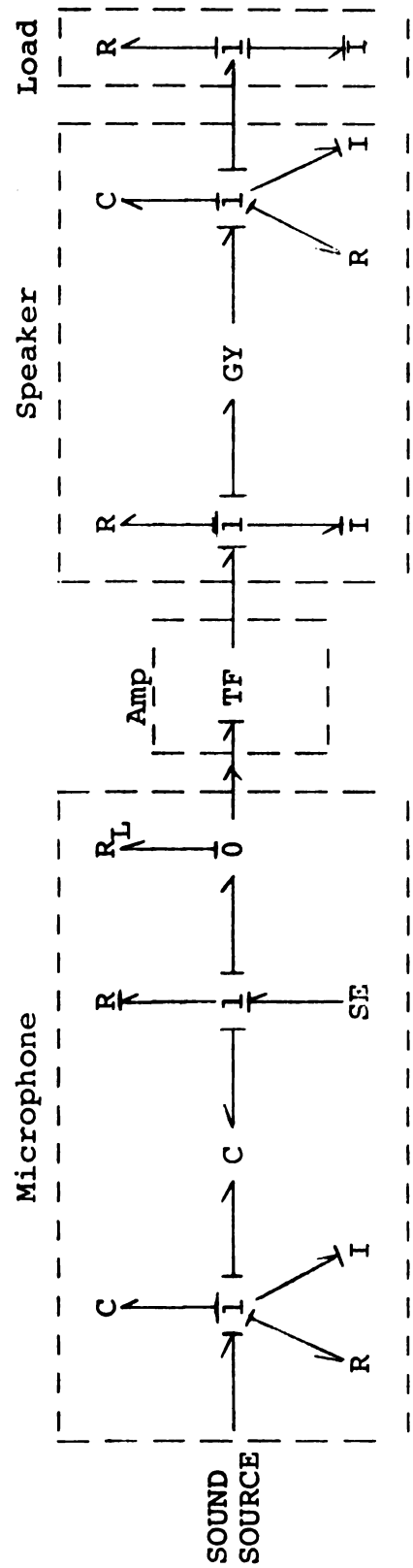

Nonlinear P.A. System Model

Figure 36

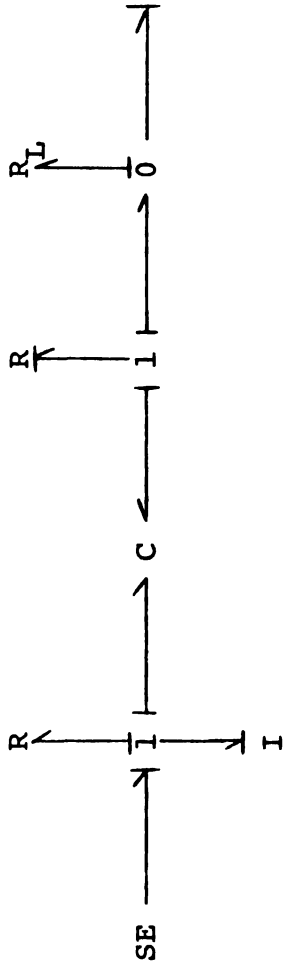

Bond Graph of Linearized Microphone

Figure 37

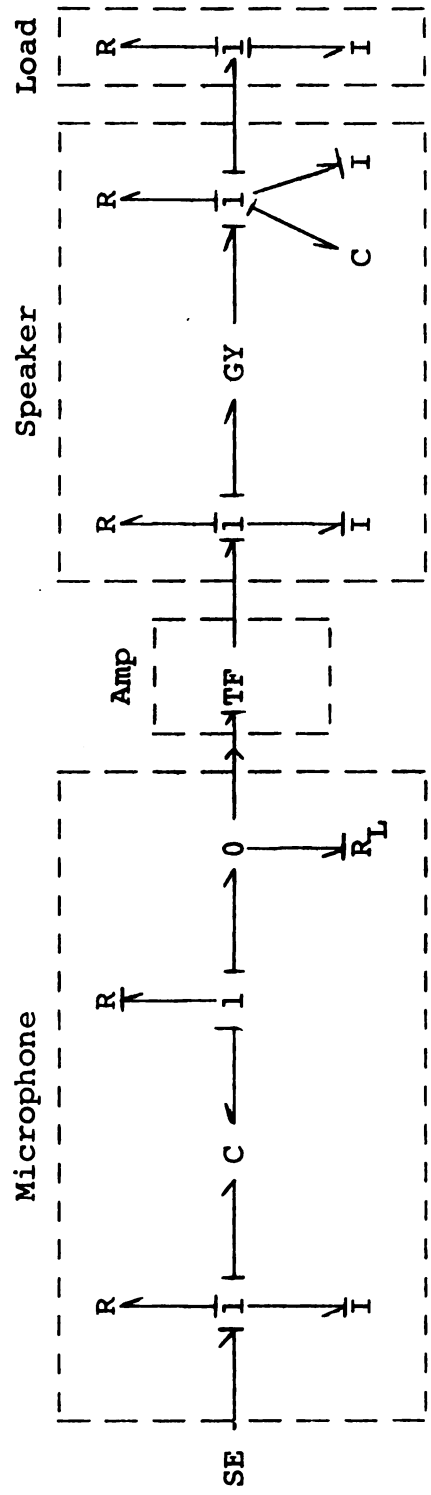

Complete P.A. System Model

Figure 38

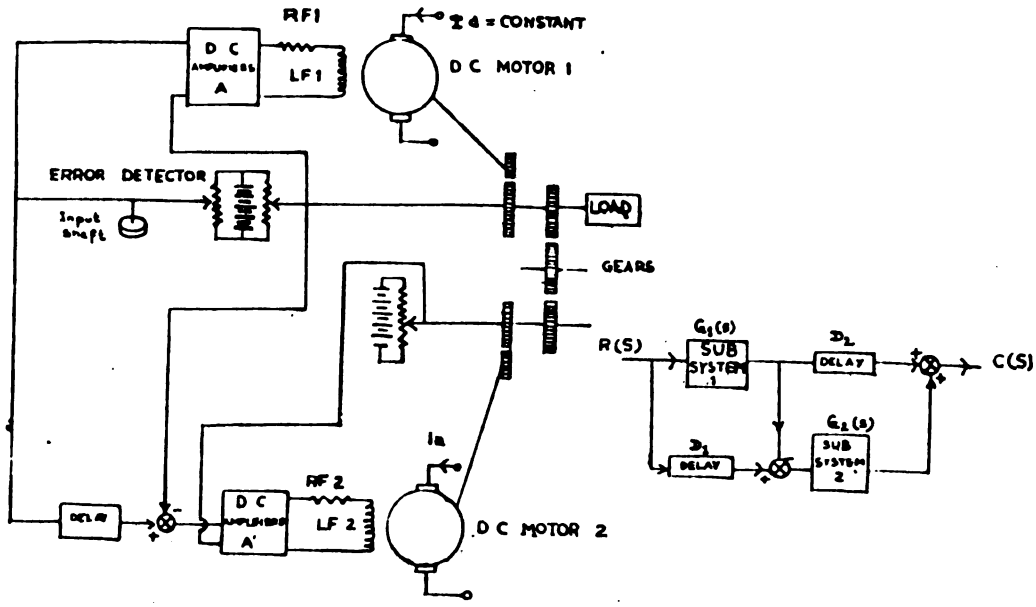

Feed Forward Position Control Schematic

Figure 39

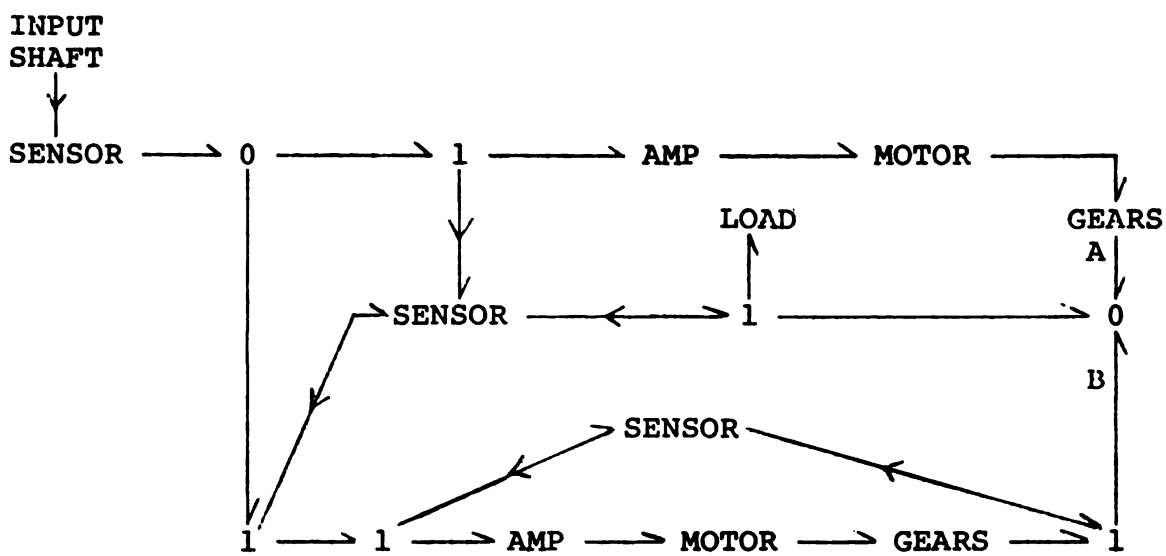

Device Level Bondgraph

Figure 40

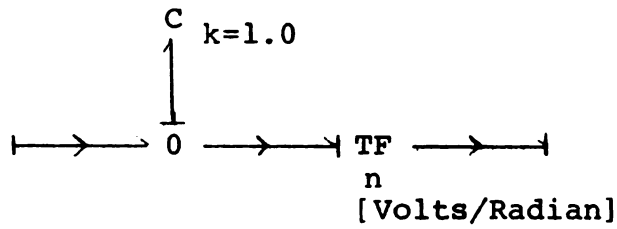

Position Sensor

Figure 41

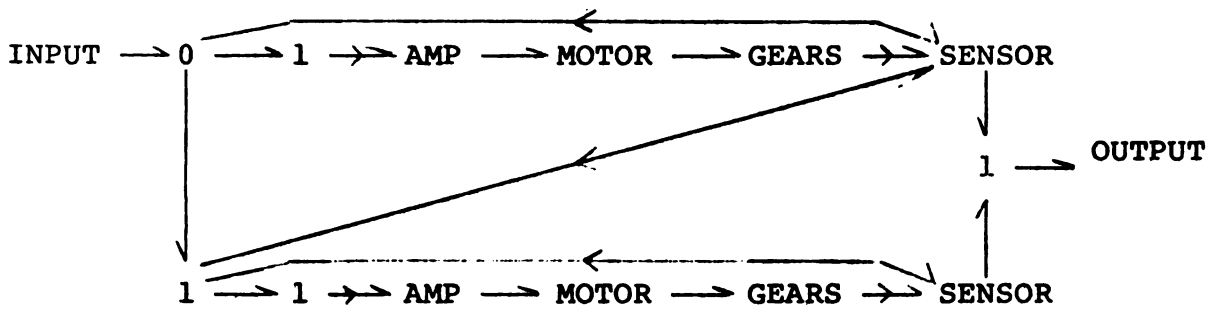

Hybrid Device Level Model

Figure 42

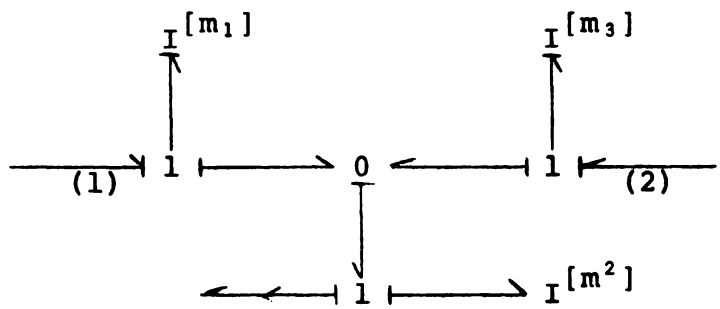

Dependent Causality

(a)

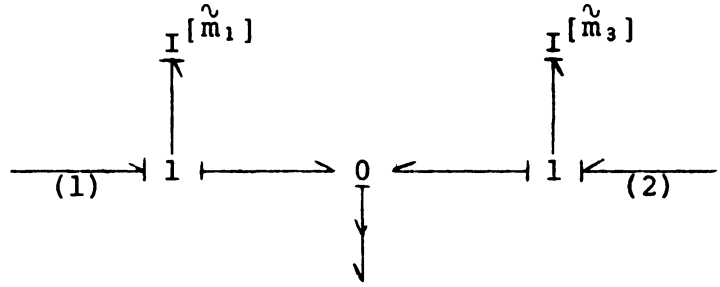

Dual Hybrid where $\tilde{m}_1$ and $\tilde{m}_3$ accound for missing m_2

(b)

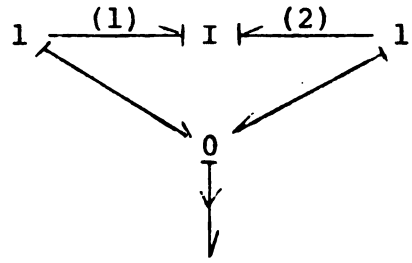

(c)

Figure 43

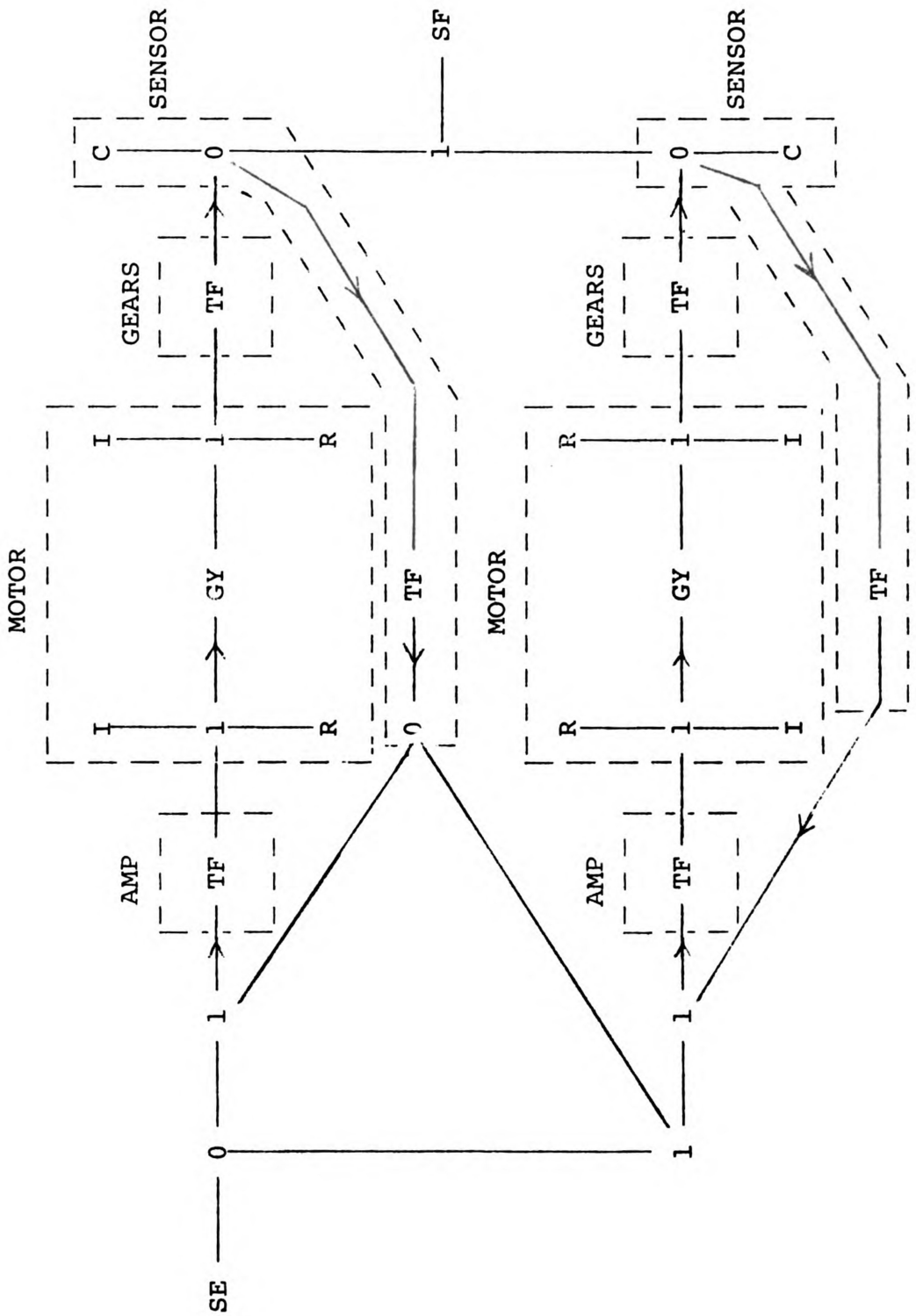

Complete Model Without Augmentation

Figure 44

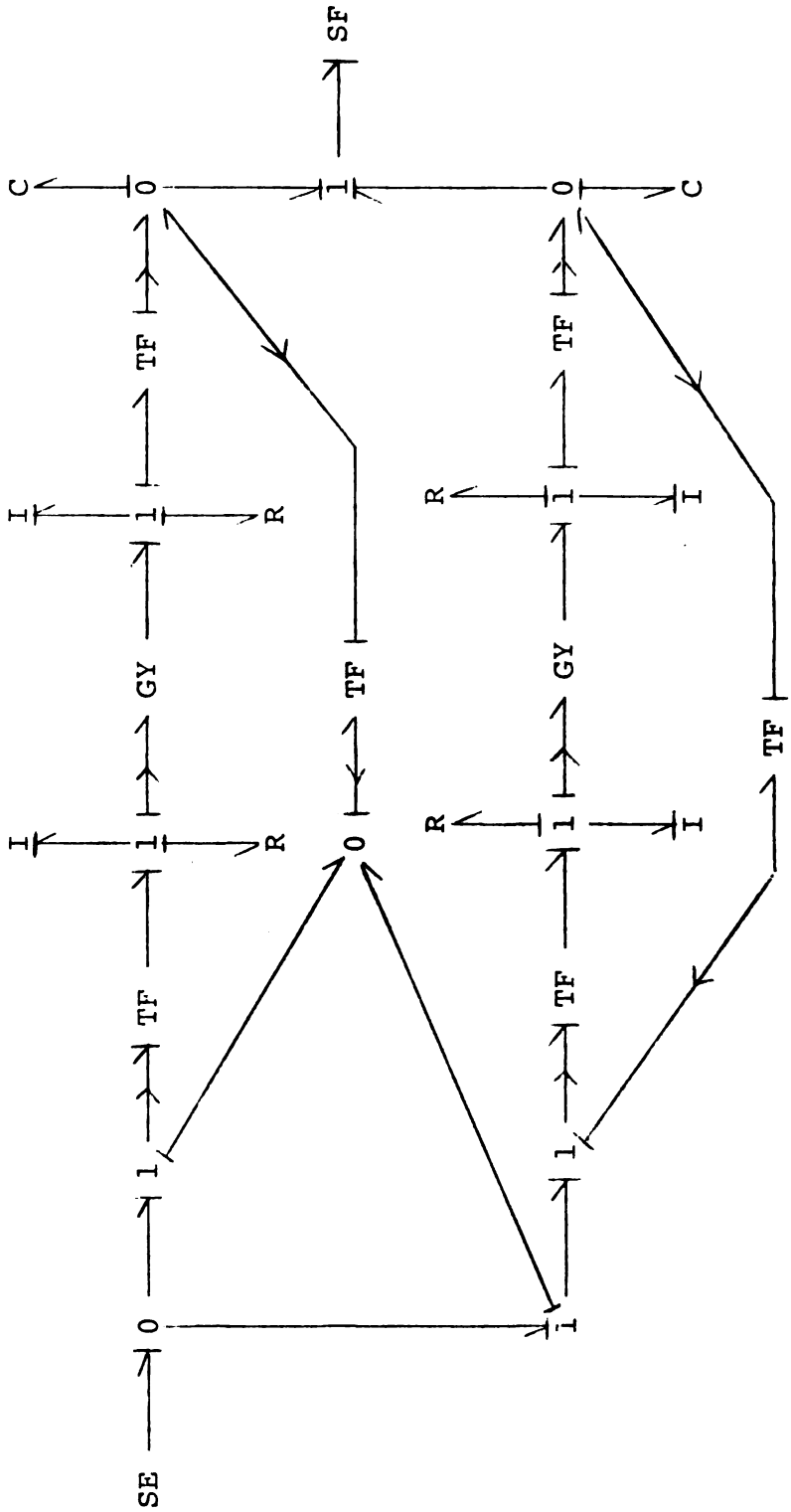

Complete Model, Fully Augmented

Figure 45

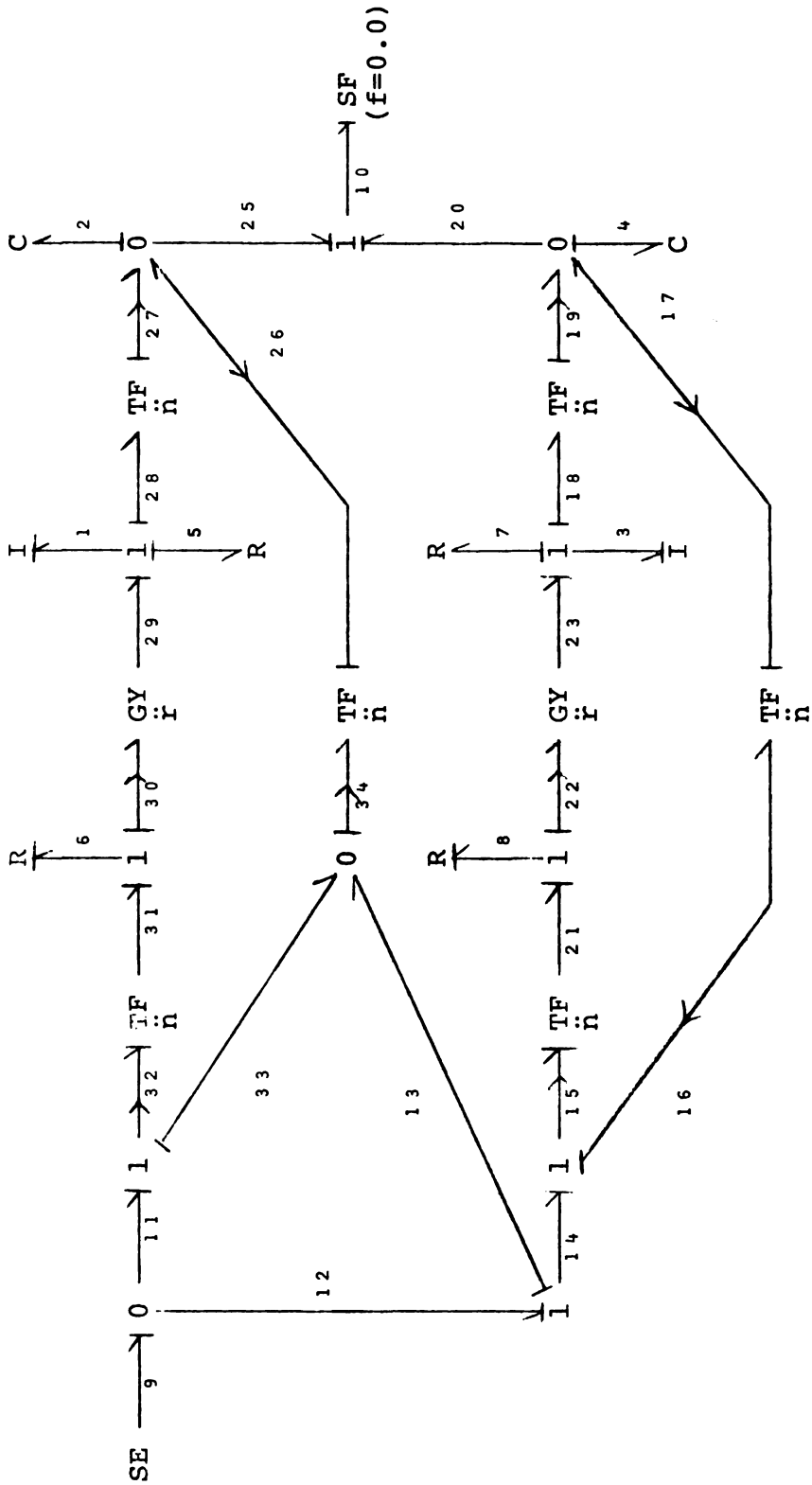

Final System Model

Figure 46

Parameter Initialization for Figure 46

$J_1 = J_2$ = Inertia of the Motor and Load = 0.001 lbm-ft/rad/sec^2

$R_5 = R_7$ = Friction of the Motor and Load = 0.001 lbf-ft/rad/sec

$n_{28-27} = n_{18-19}$ = Gear Ratio Reduction = 0.1 (i.e. $f_{28} = 10f_{27}$)

$R_6 = R_8$ = Motor Field Resistance = 5.0 ohms

$C_2 = C_4$ = Motor Velocity Integrating Constant = 1.0

$n_{34-26} = n_{16-17}$ = Sensor Sensitivity = 1.0 volt/radian

$n_{32-31} = n_{15-21}$ = D. C. Amplifier Gain = 400.0(i.e. $e_{31} = 400e_{32}$)

$r_{30-29} = r_{22-23}$ = Motor Field Constant = 0.5 lbf-ft/amp

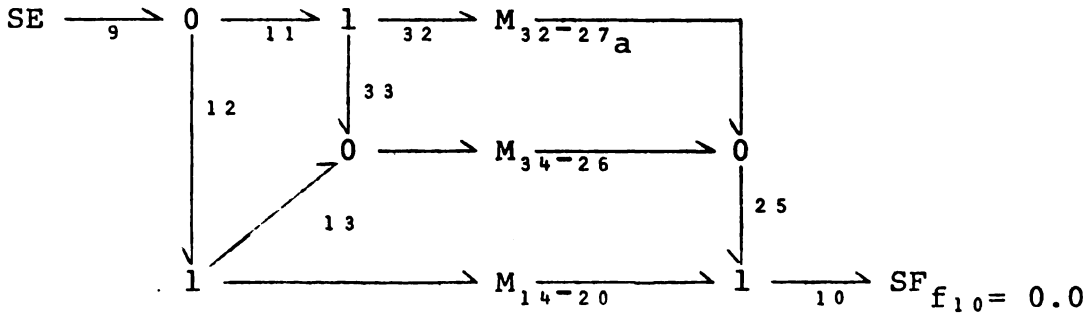

Figure 47

CATALOG

The Catalog, which is included as Appendix A, contains a representative collection of common electromechanical system components. While the component models do not represent all possible configurations, they are chosen to have considerable utility. The components are grouped by main function, (i.e., motors, sensors, etc.). Aside from general groupings, there is no other organization. As the catalog is expanded more formal organization may be required. Though consistancy of representation is attempted, it is by no means a "hallmark", due to the nature of some of the components. Where applicable, three models are presented for each component: ideal, static, and dynamic.

CONCLUSIONS

Throughout this thesis, it has been shown how the Bondgraph Multiport Approach is well-suited to the modeling of electromechanical systems. In particular, this work has demonstrated the value of modeling electromechanical systems from a component level and indicated the ease with which the components can be assembled into larger systems, which may be organized at a simple or complex level according to the engineer's needs.

In addition to the use of electromechanical components for electromechanical system models, the components can be used in conjunction with other multiport energy domains such as fluid power systems, for which an initial Component Catalog has been assembled[5].

With the development of an Electromechanical Multiport Component Catalog it is now feasible to think in terms of developing a computer library of electromechanical components. However, concerning future research and development in this area, two factors are of primary concern in order to make this approach practically useful in industrial applications. The first is the development of a large-scale electromechanical component catalog and the second is

that the Enport program must be able to handle a larger and more complex set of systems models than its current capabilities allow.

REFERENCES

(1) Karnopp, D.C. and Rosenberg, R.C. System Dynamics; A unified Approach. New York: Wiley & Sons, 1975.

(2) ASME, Journal of Dynamic Systems, Measurement, and Control. Sept. 1972.

(3) Rosenberg, R.C. A Users Guide to Enport, New York: Wiley & Sons, 1974.

(4) Charkey, E.S. Electromechanical System Components, Wiley & Sons, New York, 1972.

(5) Ray, M. The Multiport Approach to Modeling Fluid Power Systems, Michigan State University, Dept. of Mechanical Engineering, 1974, MS thesis.

(6) Evans, L.L. Simulation Techniques for the Study of Nonlinear Magnetic Field Engineering, M.I.T. Dept. of Mechanical Engineering, 1968, PhD thesis.

(7) Szabados, B.; Sinha, N.K.; d: Cenzo, C.D. A Realistic Math Model for DC Motors, Control Engineering, Mar. 1972.

(8) Crandall, Darhopp, Kurtz, and Pridmore-Brown, Dynamics of Mechanical & Electromechanical Systems. New York: McGraw-Hill, 1968.

(9) Kulkarni, S.K.; Chary, L.R., "An Objective Investigation of a Feedforward Servomechanism" I.E.E.E. Transactions on Industrial Electronics and Control Instrumentation, August 1973.

(10) Say, M.G., "Introduction to the Unified Theory of Electromagnetic Machines New York: Pitman Publishing, 1971.

APPENDIX

Catalog Contents

Sensors

- Potentiometers
- LVDT
- VACT
- Tachometer

DC Motors

- Series
- Shunt
- Permanent Magnet
- Compound

Miscellaneous

- Microphone
- Solenoid
- Amplifier
- Loudspeaker

SENSORS

Potentiometer

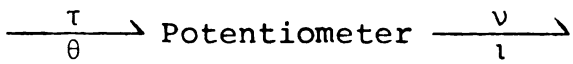

Device Level Model

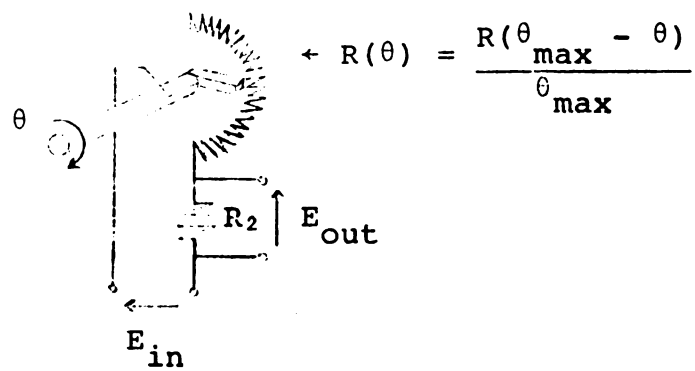

Potentiometer Schematic

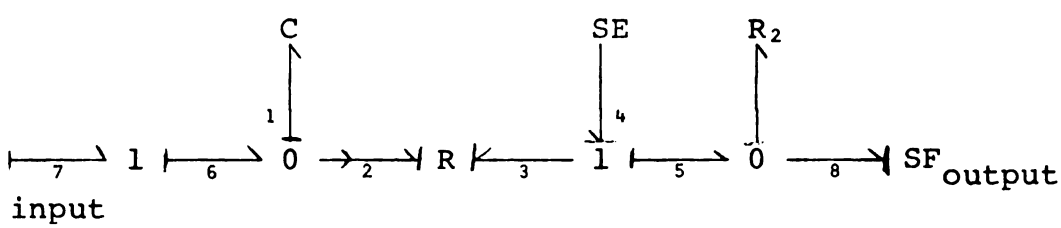

Complete Potentiometer Model

Parameter Identification - Complete Model

C_1 Velocity Integrator

$R_{2\,3}$ Modulated Resistance, $f_3 = \phi(e_3, \theta)$

R_2 Load Resistance

SE_4 Circuit Voltage

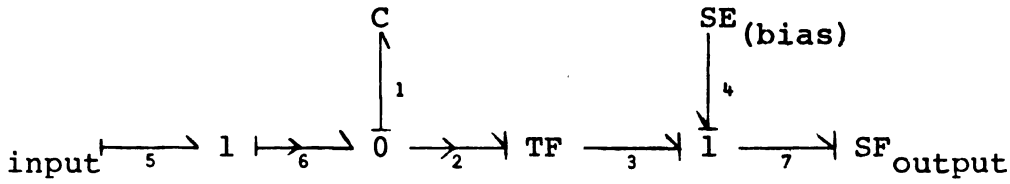

Simplified Potentiometer Model*

Parameter Identification - Simplified Model

C_1 Velocity Integrator

TF_{23} Transformer (volts/radian)

SE_4 Bias Boltage

$$\{E_4 = \frac{R_2 E_{IN}}{R(\theta=0) + R_2}\}$$

LVDT (Linear Variable Differential Transformer)

$$\frac{F}{\dot{x}} \rightarrow \text{L.V.D.T.} \rightarrow \frac{v}{1}$$

Device Level Model

Schematic of LVDT

---

*Suitable within the following conditions:

for $R(\theta) = \frac{R(\theta_{max} - \theta)}{\theta max}$: $0 < \theta \lesssim .6\theta$ $R \gg R_2$

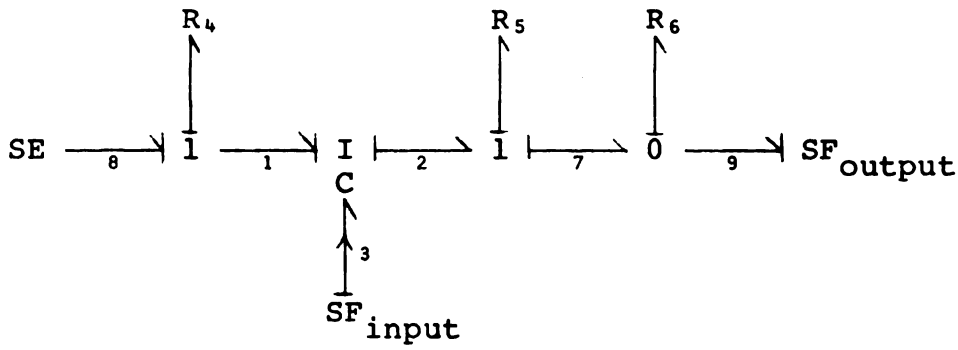

Complete LVDT Model

Parameter Identification - Complete

IC_{123} Inductance of Primary and Secondary Coils combined with the Capacitance effect from the Ferromagnetic Core

$\iota_1 = \phi_1(\lambda_1, \lambda_2, x)$

$\iota_2 = \phi_2(\lambda_1, \lambda_2, x)$

R_4 Primary Coil Resistance

R_5 Secondary Coil Resistance

R_6 Load Resistor

SE_8 Bias Voltage

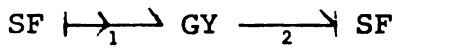

Simplified LVDT Model

GY_{12} Gyrator (r - scaling factor, volts/rad/sec)

Variable Area Capacitive Transducer

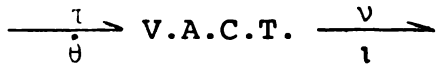

Device Level Model

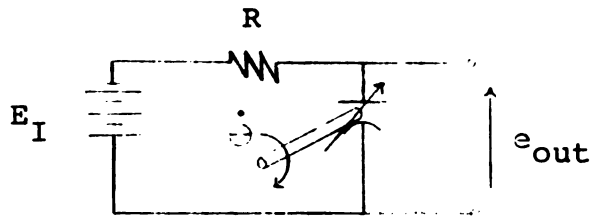

V.A.C.T. Schematic

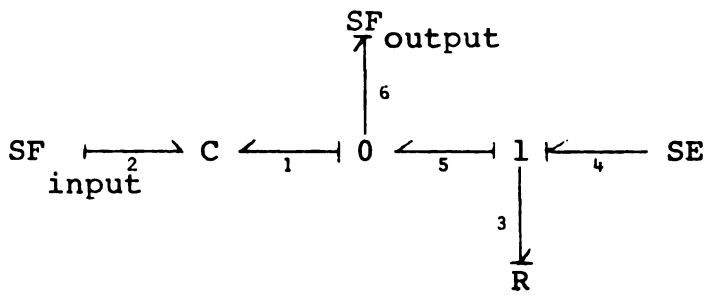

Complete Capacitive Transducer Model

Parameter Identification - Complete Model

C_{12} Modulated Capacitance $e_1 = \phi(q,\theta)$

R_3 Electrical Resistance

SE_4 Constant Voltage (E_I)

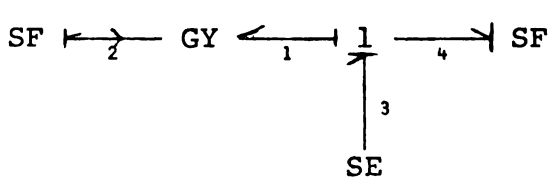

Simplified Capacitive Transducer Model*

---

*where $C(\theta) = \frac{\varepsilon A}{d}(\theta_0 + \theta)$ and

$$\left|\frac{\varepsilon A R_3}{d}\dot{\theta}(t)\right| \ll 1$$

Parameter Identification - Simplified Model

GY_{12} Gyrator Scales e_1 to $\dot{\theta}$

SE_3 Bias Voltage, E_I

Tachometer

Device Level Model

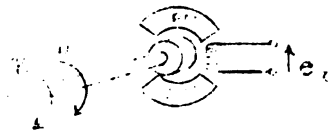

Tachometer Schematic

Ideal Tachometer Model

GY_{12} Gyrator (r-scale factor, volts/radian/sec)

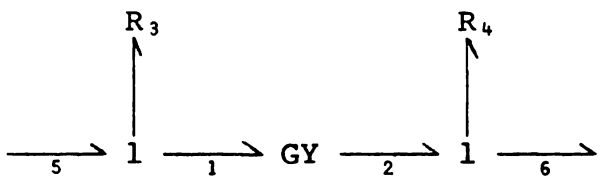

Static Tachometer Model

GY_{12} Electromagnetic Field Effect, Gyrator

R_3 Electrical Resistance

R_4 Mechanical Damping

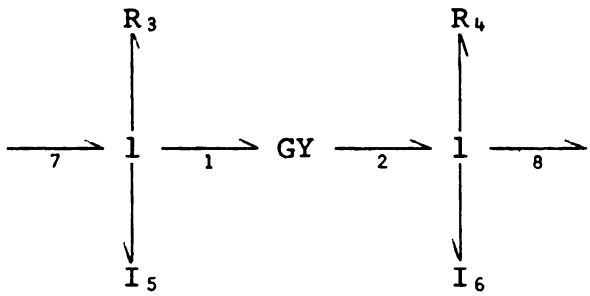

Dynamic Tachometer Model

GY_{12} Gyrator, Electromagnetic Field Effect

R_3 Electrical Resistance

R_4 Mechanical Damping

I_5 Electrical, Armature Inductance

I_6 Mechanical, Rotary Inertia

DC MOTORS

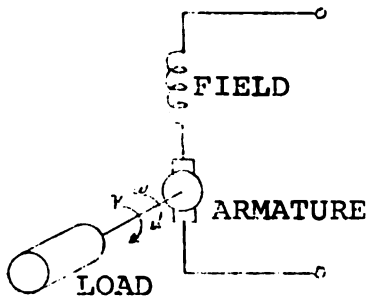

SERIES

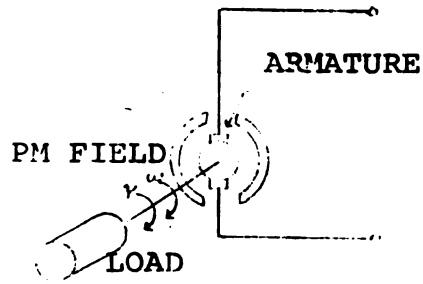

PERMANENT MAGNET

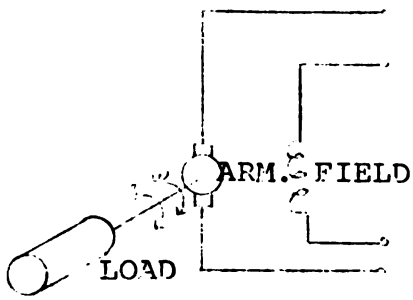

SHUNT

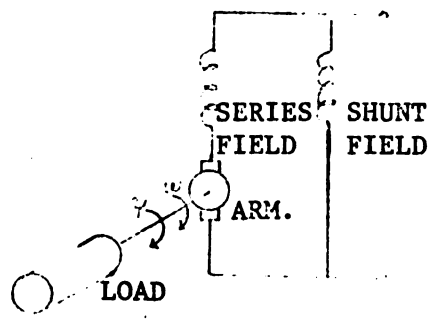

COMPOUND

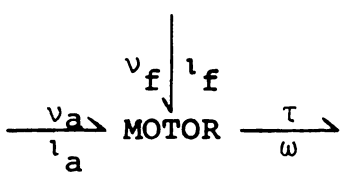

Word Bond Graph

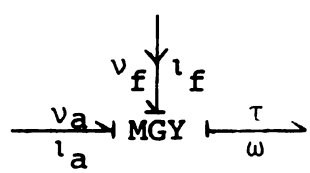

General Ideal Motor Model

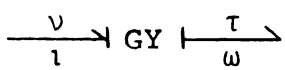

Ideal Linear Motor Model

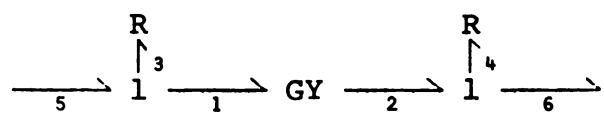

Static Motor Model

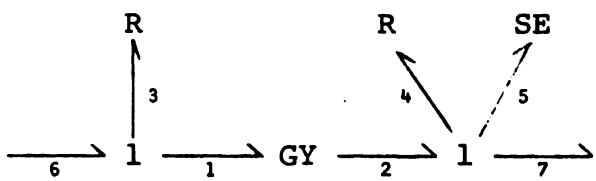

Piecewise Linear Static Model

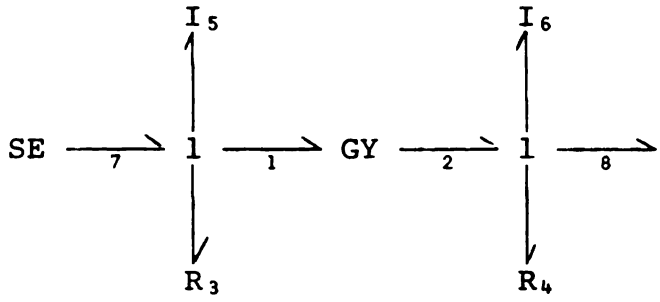

Dynamic PM Motor Model

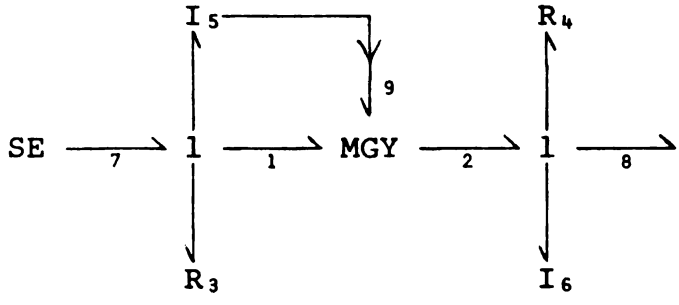

Dynamic Series Motor Model

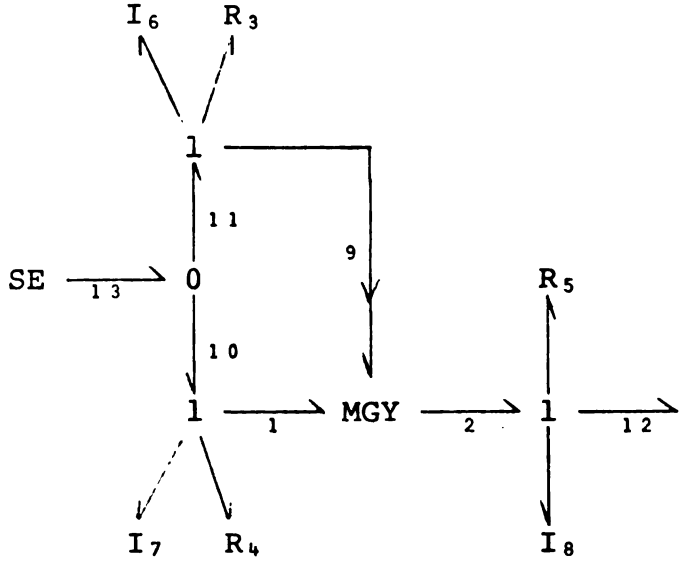

Dynamic Shunt Motor Model

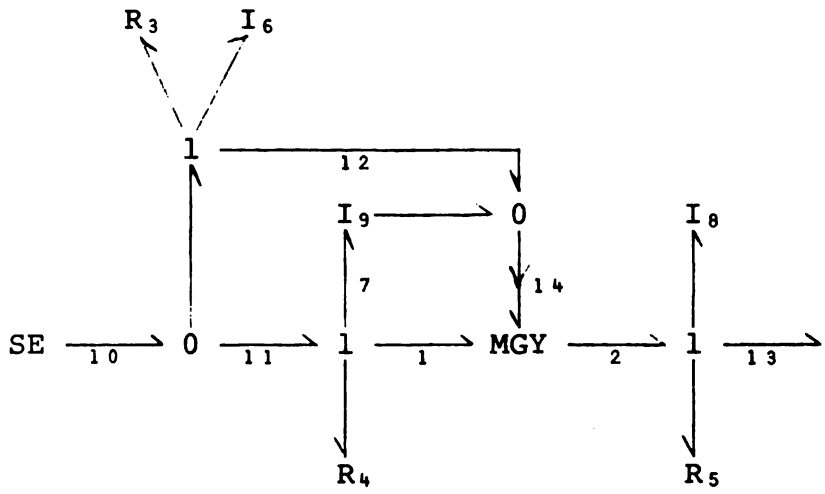

Dynamic Compound Motor Model

Parameter Identification

Static Motor Model

GY_{12} Gyrator, Electromagnetic Field Effect

R_3 Armature Electrical Resistance

R_4 Mechanical Damping

Piecewise Linear Static Model

GY_{12} Gyrator, Electromagnetic Field Effect

R_3 Armature Electrical Resistance

R_4 Air Friction Damping

SE_5 Bearing Friction where E_5 = sign(velocity)*|constant|

Dynamic Permanent Magnet Motor Model

GY_{12} Gyrator, Electromagnetic Field Effect

R_3 Armature Resistance

R_4 Mechanical Damping

I_5 Armature Inductance

I_6 Mechanical Rotary Inertia

SE_7 Command Voltage

Parameter Identification - Continued

Dynamic Series Motor Model

MGY_{129} Modulated Gyrator, Nonlinear Electromagnetic Field Effect

R_3 Armature and Field Resistance

R_4 Mechanical Damping

I_{59} Armature and Field Inductance

I_6 Mechanical Rotary Inertia

SE_7 Command Voltage

Dynamic Shunt Motor Model

MGY_{129} Modulated Gyrator, Nonlinear Electromagnetic Field Effect

R_3 Field Resistance

R_5 Mechanical Damping

I_6 Field Inductance

I_7 Armature Inductance

I_8 Mechanical Rotary Inertia

SE_{13} Command Voltage

Dynamic Compound Motor Model

MGY_{1214} Modulated Gyrator, Nonlinear Electromagnetic Field Effect

R_3 Shunt Field Resistance

R_4 Series Field and Armature Resistance

R_5 Mechanical Damping

I_6 Shunt Field Inductance

Parameter Identification - Continued

I_θ Mechanical Rotary Inertia

SE_{10} Command Voltage

Microphone

Device Level Model

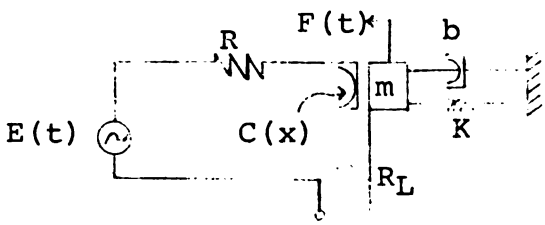

Microphone Schematic

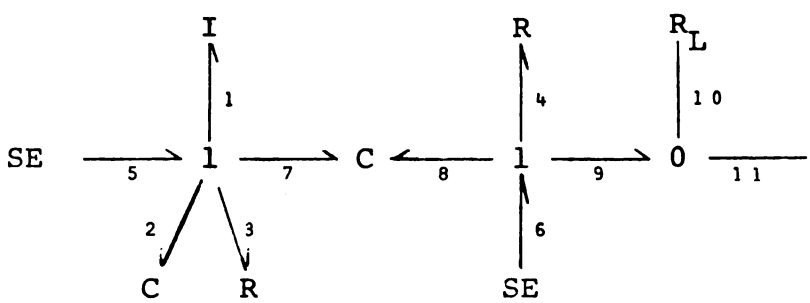

Complete Nonlinear Microphone Model

Parameter Identification - Complete Model

C_{78} Moving Plate Capacitance $F_7 = \phi_1(q_8, x_7), F_8 = \phi_2(q, x)$

I_1 Mass of Moving Plate

C_2 Mechanical Compliance of Moving Plate

R_3 Mechanical Damping

R_4 Electrical Circuit Resistance

SE_6 Bias Voltage

R_L Load Resistor

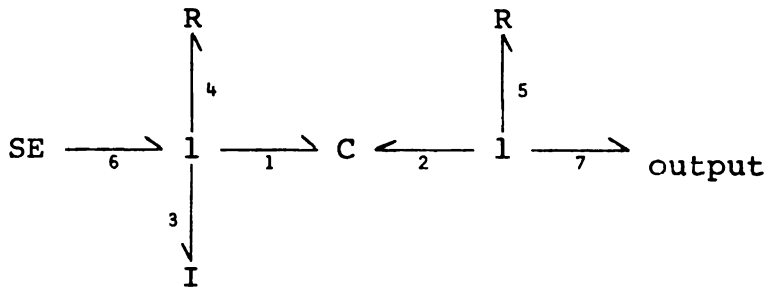

Complete Linear Microphone Model

Parameter Identification - Linearized Model

C_{12} Linearized Capacitance and Compliance

I_3 Mass of Moving Plate

R_4 Mechanical Damping

R_5 Electrical Resistance

Solenoid

Device Level Model

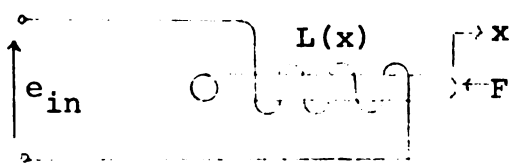

Solenoid Schematic

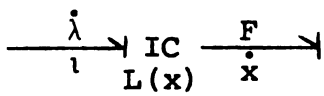

Ideal Solenoid Model

Parameter Identification - Ideal

IC Electrical Inductance and Mechanical Capacitance of Moveable Core Inductor

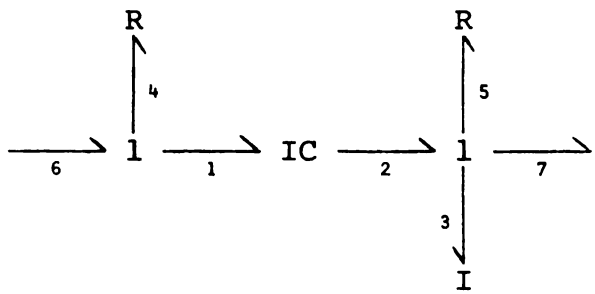

Complete Solenoid Model

Parameter Identification - Complete

IC_{12} Same as above, $F = \phi_1(\lambda,x)$, $\imath = \phi_2(\lambda,x)$

I_3 Mass of Core

R_4 Electrical Circuit Resistance

R_5 Mechanical Damping

Amplifier

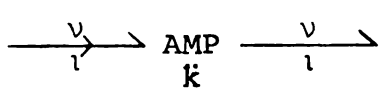

Device Level Model

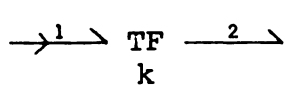

Ideal Linear Amplifier Model

Parameter Identification - Ideal Linear

TF_{12} Transformer, k-Gain

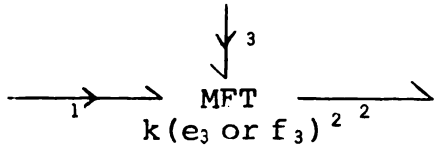

Ideal Nonlinear Amplifier Model

Parameter Identification - Ideal Nonlinear

$MTF_{1\,2\,3}$ Modulated Transformer, k-Gain Determined by Signal of Bond 3

Loudspeaker

Device Level Model

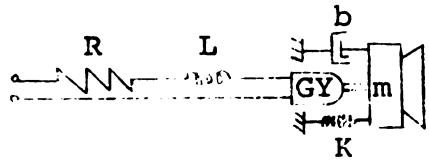

Loudspeaker Schematic

Ideal Speaker Model

Parameter Identification - Ideal Model

$GY_{1\,2}$ Gyrator, Electormagnetic Field Effect

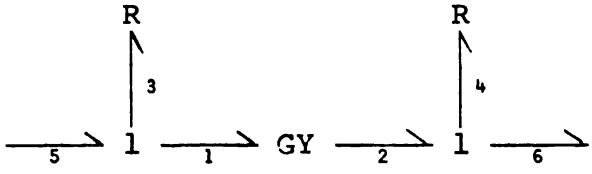

Static Speaker Model

Parameter Identification - Static Model

GY_{12} Gyrator, Electromagnetic Field Effect

R_3 Electrical Resistance

R_4 Mechanical Damping

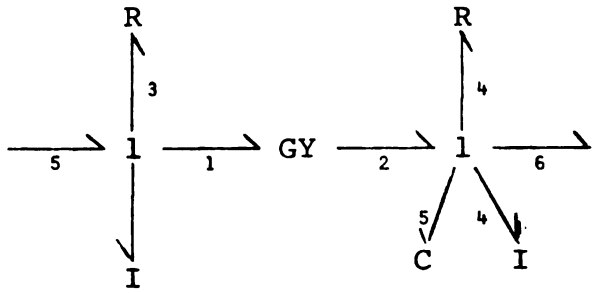

Dynamic Speaker Model

Parameter Identification - Dynamic Model

GY_{12} Gyrator, Electromagnetic Field Effect

I_3 Electrical Inductance of Voice Coil

I_4 Mass of Speaker

C_5 Compliance of Speaker

R_6 Mechanical Damping of Speaker

R_7 Electrical Circuit Resistance